Journal for ImmunoTherapy of Cancer

Functional analysis of peripheral and intratumoral neoantigen-specific TCRs identified in a patient with melanoma

Eva Bräunlein ,[1] Gaia Lupoli,[1] Franziska Füchsl ,[1] Esam T Abualrous,[2] Niklas de Andrade Krätzig,[3,4] Dario Gosmann ,[1] Lukas Wietbrock,[5] Sebastian Lange ,[3,4,6] Thomas Engleitner ,[3,4] Huan Lan,[2] Stefan Audehm,[1] Manuel Effenberger,[7] Melanie Boxberg ,[8,9] Katja Steiger ,[8,10,11] Yinshui Chang,[1] Kai Yu,[1] Cigdem Atay,[1,11] Florian Bassermann ,[1,4,11] Wilko Weichert ,[8,9,10,11] Dirk H Busch ,[7] Roland Rad ,[3,4,6,11] Christian Freund ,[2] Iris Antes ,[5] Angela M Krackhardt [1,4,11]

To cite: Bräunlein E, Lupoli G, Füchsl F, *et al*. Functional analysis of peripheral and intratumoral neoantigen-specific TCRs identified in a patient with melanoma. *Journal for ImmunoTherapy of Cancer* 2021;**9**:e002754. doi:10.1136/jitc-2021-002754

► Additional supplemental material is published online only. To view, please visit the journal online (http://dx.doi.org/10.1136/jitc-2021-002754).

EB and GL are joint first authors.

Accepted 03 August 2021

For numbered affiliations see end of article.

Correspondence to
Professor Angela M Krackhardt; angela.krackhardt@tum.de

ABSTRACT

Background Neoantigens derived from somatic mutations correlate with therapeutic responses mediated by treatment with immune checkpoint inhibitors. Neoantigens are therefore highly attractive targets for the development of therapeutic approaches in personalized medicine, although many aspects of their quality and associated immune responses are not yet well understood. In a case study of metastatic malignant melanoma, we aimed to perform an in-depth characterization of neoantigens and respective T-cell responses in the context of immune checkpoint modulation.

Methods Three neoantigens, which we identified either by immunopeptidomics or in silico prediction, were investigated using binding affinity analyses and structural simulations. We isolated seven T-cell receptors (TCRs) from the patient's immune repertoire recognizing these antigens. TCRs were compared in vitro by multiparametric analyses including functional avidity, multicytokine secretion, and cross-reactivity screenings. A xenograft mouse model served to study in vivo functionality of selected TCRs. We investigated the patient's TCR repertoire in blood and different tumor-related tissues over 3 years using TCR beta deep sequencing.

Results Selected mutated peptide ligands with proven immunogenicity showed similar binding affinities to the human leukocyte antigen complex and comparable disparity to their wild-type counterparts in molecular dynamic simulations. Nevertheless, isolated TCRs recognizing these antigens demonstrated distinct patterns in functionality and frequency. TCRs with lower functional avidity showed at least equal antitumor immune responses in vivo. Moreover, they occurred at high frequencies and particularly demonstrated long-term persistence within tumor tissues, lymph nodes and various blood samples associated with a reduced activation pattern on primary in vitro stimulation.

Conclusions We performed a so far unique fine characterization of neoantigen-specific T-cell responses revealing defined reactivity patterns of neoantigen-specific TCRs. Our data highlight qualitative differences of these TCRs associated with function and longevity of respective T cells. Such features need to be considered for further optimization of neoantigen targeting including adoptive T-cell therapies using TCR-transgenic T cells.

INRODUCTION

Cancer immunotherapy has demonstrated high efficacy in the treatment of diverse malignant diseases as shown by the potency of immune checkpoint modulation.[1] These therapies can unleash antitumor immune responses by conveying recognition and eradication of cancers by the patients' own immune system, although the contribution of specific T cells and the targeted antigens are not predefined. However, not all patients benefit from this therapeutic approach, thus, understanding the nature of tumor recognition versus escape remains of fundamental importance for the development of novel immunotherapeutic approaches and the improvement of patients' outcomes. The tumor mutational load is an important prognostic and predictive biomarker for the therapeutic success of immune checkpoint inhibitors across various disease entities, emphasizing the role of neoepitopes in tumor recognition and rejection.[2] Moreover, identification and characterization of neoantigens and neoantigen-specific T-cell responses are of particular interest for the generation of new personalized immunotherapies, such as vaccination and cellular therapies.[3–5] In order to fully exploit the potential of neoantigen-directed immunotherapy, more efforts are required to understand different qualities of neoepitopes and their respective T-cell receptors (TCRs) specifically recognizing them. We believe that case studies are currently a valid source to investigate the multitude of aspects

involved[6] and that more detailed, comprehensive data are necessary to this purpose. Recently, we have identified two neoantigens by mass spectrometry (MS) and validated these by proof of defined neoantigen-specific autologous T-cell responses in a patient with melanoma.[7] We have now extended the number of immunogenic antigens in this patient using additional prediction analyses and characterized neoantigens by 3D modeling as well as experimental validation of major histocompatibility complex (MHC)–peptide stability. In addition, we identified seven TCRs recognizing these antigens. We tracked these TCRs in blood and different tissues of the patient over time and functionally characterized them in vitro as well as in vivo, providing evidence of substantial differences regarding functionality and longevity with relevance for further comprehensive immunotherapies.

MATERIALS AND METHODS

Primary human specimens and cell lines

An overview of the clinical course of the patient with melanoma is given in online supplemental figure 1, as well as in online supplemental material and methods in more detail. All resected samples were handled as previously described for confirmation of diagnosis and expansion of tumor-infiltrating lymphocytes (TILs) from a lung metastasis (M_{Lung}).[7] Peripheral blood mononuclear cells (PBMCs) were isolated by density-gradient centrifugation (Ficoll-Hypaque, Biochrom) immediately on receipt using EDTA-anticoagulated blood from the patient and blood or apheresis products from healthy donors followed by storage in liquid nitrogen.

PBMCs and T cells used for experiments were cultivated as previously described.[7] $CD8^+$ T cells used for transduction were obtained by magnetic separation from healthy donor-derived apheresis products (Dynabeads Untouched Human $CD8^+$ T Cells Kit, Thermo Fisher; Magnet, DynaMag).

Cell lines used in this study were T2 (American Type Culture Collection - ATCC cat# CRL-1992), purchased from ATCC in 2005; lymphoblastoid cell lines (LCLs) HOM-2 (European Collection of Authenticated Cell Cultures - ECACC cat# 98092902), SWEIG007 (ECACC cat# 88052037), AMALA (Interlab Cell Line Collection - ICLC cat# HTL14002), OZB (ECACC cat# 94022545), RSH (ECACC cat# 88052021), KLO (ECACC cat# 94050324), LWAGS (ECACC cat# 88052078), and BM21 (ECACC cat# 88052043), kindly provided by Steve Marsh in 2007; human metastatic melanoma cell line A2058 (ECACC cat# 91100402) and human colon carcinoma cell line MDST8 (ECACC cat# 99011801) purchased from Sigma-Aldrich in 2018; B-cell lymphoma cell line U-698-M (DSMZ cat# ACC-4), acquired from Deutsche Sammlung von Mikroorganismen und Zellkulturen (DSMZ) in 2018; embryonal kidney cell line 293Vec-RD114 (BioVec Pharma, Québec, Canada); and NS0-IL15, kindly provided by S. R. Riddell in 2011.[8] LCL (LCL8) was generated in our laboratory by infection and immortalization of healthy donor-derived B cells with Epstein-Barr virus-containing supernatant in 2011. Absence of mycoplasma infection in cell line cultures was routinely confirmed by PCR (Venor GeM mycoplasma detection kit, Minerva Biolabs). Culture conditions are described in online supplemental material and methods.

DNA extraction, exome and TCR-β sequencing

For exome and T-cell receptor beta (TCR-β) deep sequencing, genomic DNA (gDNA) was extracted from a lung biopsy (B_{Lung}), an intestinal metastasis (M_{Int}), M_{Lung} and draining lymph nodes (LNs) after microdissections of respective regions of interest. The extraction of nucleic acids was performed on 2 µm formalin-fixed, paraffin-embedded (FFPE) tissue slides using Maxwell RSC Blood DNA Kit (Promega) following the manufacturer's recommendations. DNA was extracted from PBMCs obtained from diverse blood withdrawals (online supplemental figure 1) and M_{Lung}-derived TILs with DNeasy Blood & Tissue Kit (Qiagen). Whole-exome sequencing and single-nucleotide variant (SNV) analyses from M_{Int} were available from our previous publication and were afterwards obtained for M_{Lung}, as previously described.[7] Next-generation sequencing of TCR-β loci was performed by Adaptive Biotechnologies with ImmunoSEQ platform at the deep level (exception made for B_{Lung} gDNA, which underwent TCR-β sequencing survey level only due to limited material).

In silico prediction of peptide ligands and human leukocyte antigen (HLA) binding affinity

Putative mutated nonamer peptide ligands originating from SNVs, identified through a stringent variant calling approach,[7] were predicted by translating all sequences bearing a mutation to 23-residue long amino acid (AA) sequences (mutated AA in 12th position). Protein transcripts were downloaded from Ensembl GRCh38, release 86. In cases where the mutation was located less than 12 AA from the 3′ or 5′ terminus of the gene, the string was shorter and the mutation was not centrally located. Peptide–HLA class I binding affinity was predicted for the patient's HLA alleles HLA-A03:01 and HLA-B27:05 using NetMHC V.4.0. Nonamer peptides were ranked by predicted affinity (cut-off <500 nM) (online supplemental tables 1 and 2). Half maximal inhibitory concentration (IC_{50}) in vitro measurements were performed as described in online supplemental material and methods.

Immunogenicity assessment of mutated peptide ligands

For immunogenicity assessment, peptide ligands were ordered from Genscript and DgPeptides. Ligands identified by MS, including $NCAPG2^{P333L}$ and $SYTL4^{S363F}$, were tested for recall antigen-experienced T-cell responses as described in the online supplemental material and methods. Predicted peptides were arranged in pools according to predicted affinity (online supplemental table 3) and in vitro screened for immunogenicity following protocols described in the online supplemental

material and methods. Reactivity was assessed by specific Interferon-gamma (IFN-γ) release by ELISpot assay by coating ELISpot plates (MAHAS4510) with IFN-γ capture antibody (MABTECH cat# 3420-3-250) followed by application of IFN-γ-detection antibody (MABTECH cat# 3420-6-250) and visualization by streptavidin–horseradish peroxidase (MABTECH cat# 3310-9-1000).

Structural modeling of neoantigen binding to respective HLA complexes

Neoantigens and wild-type (WT) peptides were modeled on experimental structures of HLA-A03:01 (PDB-ID: 2XPG)[9] and HLA-B27:05 (PDB-ID 1W0V)[10] crystallized with nine AA long ligands. Peptides from the template were mutated into neoantigen/WT sequences using the IRECS program.[11]

Solvent-accessible surface area (SASA) values were calculated using the VMD software V.1.9.2,[12 13] applying a probe radius of 1.4 Å. Further information is provided in online supplemental materials and methods. Details about heat-up parameters are provided in online supplemental table 4.

Flow cytometry-based assessment of TCR expression

Transduction efficiency was determined by staining of transgenic TCR using an antibody specifically binding to murine TCR constant beta chain (TCRmu-antibody (clone H57-597), Thermo Fisher Scientific cat# 11-5961-81) based on the isotype control (Thermo Fisher Scientific cat# 11-4888-81). For multimer staining, Strep-tagged mutated and WT peptide-Human Leucocyte Antigen (pHLA) (eg. SYTL4^{S363F} and SYTL4^{WT}) were multimerized on a fluorophore labeled Strep-Tactin backbone (Iba GmbH) in a 1 µg:1 µL ratio. Transduced T cells were stained with multimers, anti-CD8 (BD Biosciences cat# 557085 and BD Biosciences cat# 555634), anti-CD3 (BD Biosciences cat# 557694) and 7-aminoactinomycin D. All flow cytometry measurements were performed with LSRII or LSRFortessa flow cytometers (BD Biosciences) and analyzed with FlowJo Software V.10.

Functional analyses of TILs and TCR-transgenic effector T cells

TCR-transduced T cells were coincubated with target cells (LCL-1) transduced with different minigene (MG) constructs or pulsed with defined peptides (1 µM). WT MGs and/or irrelevant peptides served as controls for TCR specificity. Assays for detection of cytokine secretion were performed in triplicate (effector to target (E:T)=1:1; 10,000 target and effector cells per well). Supernatants from T-cell cultures were used for assessment of a diverse cytokine panel with MACSPlex 12 Cytokines Kit (Miltenyi Biotech) following the manufacturer's recommendations. Reactivity of TILs was assessed by IFN-γ ELISpot assay on a coculture with autologous peptide-pulsed γ-irradiated LCLs (1 µM) for 24 hours using at E:T of 1:1.

Functional avidity was assessed by incubating transgenic T cells with T2 target cells (ATCC CRL-1992) pulsed with titrated peptide concentrations (E:T=1:1; 10,000 cells/well). IFN-γ secretion was quantified by ELISA, and values obtained were fitted into a non-linear variable-slope regression curve on GraphPad Prism V.7.

Functional avidity assays were performed at least three times using at least two different transductions and donors showing comparable results.

In vitro target cell killing was assessed by impedance-based xCELLigence assays as described in online supplemental material and methods.

TCR cross-reactivity was tested by stimulation of TCR-transgenic T-cell populations with T2 cells pulsed with ala/thr substitution variants of the three neoepitopes, in direct comparison to the original mutated identified peptides. IFN-γ values from every condition were normalized on the positive control using the following formula:

$$IFN-\gamma\ \text{secretion}\ (\%) = \frac{IFN-\gamma\ \text{secretion}\ (\text{ala/thr})\left[\frac{pg}{ml}\right]\times 100}{IFN-\gamma\ \text{secretion}\ (\text{mutated peptide})\left[\frac{pg}{ml}\right]}$$

Relative IFN-γ-secretion after incubation with an ala/thr variant above 50% was considered as a replaceable position.

For cross-reactivity scan of synthesized peptides based on the ScanProsite pattern, T cells were coincubated with T2 cells pulsed with 1 µM of peptide (E:T=1:1; 10,000 cells/well). Analysis was conducted for at least two different donors for each TCR construct.

For evaluation of general alloreactivity, TCR-transduced T cells were stimulated with respective neoantigens presented in the context of different HLA class I alleles as well as non-pulsed target cells. Effector cells were cultured with LCL presenting a broad variety of HLA alleles (online supplemental table 5), pulsed with mutated peptides (E:T=1:1; 10,000 cells/well). As readout, IFN-γ production was quantified by ELISA.

In vivo TCR rejection potential

NOD.CG-Prkdc^{scid} IL2rg^{tm1Wjl}/SzJ (NSG, The Jackson Laboratory) was maintained according to the institutional guidelines and approval of local authorities. A xenograft murine model was generated as previously described.[14 15] NSG mice at the age of 6–19 weeks were subcutaneously injected with U-698-M cells (10×10^6 cells/flank) transduced with tandem MG constructs coding for defined neoantigens. Animal well-being was assessed daily and growth was monitored in vivo by external measurements with digital caliper. Ten days after administration of tumor cells, almost all mice developed visible and measurable tumor growth. T cells transduced with TCRs KIF2C-PBC1, KIF2C-PBC2, SYTL4-PBC1, SYTL4-TIL1, or a control TCR 2.5D6 targeting an irrelevant antigen (myeloperoxidase)[14] were injected intravenously. TCR-transduced T cells (2×10^7) in total were administrated to eight mice per group (n=8) over 2 days, except for KIF2C-PBC1, of which 4.6×10^6 TCR-transduced T cells were injected in total due to lower transduction efficiency. Male and female animals

as well as animals of different ages were distributed evenly across all treatment groups. Tumor growth kinetics were monitored daily for 26 days with digital caliper. Interleukin (IL)-15-producing NS0 cells ($1.0–1.5\times10^7$) were administered intraperitoneally two times per week after irradiation with 80 Gy.[16] On day 4, after the first T-cell injection, two mice per group were removed for flow cytometry analysis. On day 20, remaining tumors, bone marrow and spleen were retrieved and passed through a cell strainer. Blood samples were taken and anticoagulated with EDTA. Ammonium–chloride–potassium lysis (Life Technologies) was performed on blood samples. Single-cell suspensions were stained for detection of transgenic T cells by flow cytometry as explained previously.

Statistical analysis

Significance of differences within half maximal effective concentration (EC_{50}) values of analyzed TCRs were investigated by one-way analysis of variance (ANOVA) and Tukey's multiple comparison test. With regard to in vivo rejection potential of the TCRs, differences in tumor growth were calculated with two-way ANOVA test (time and treatment) and Dunnett's test for multiple comparisons. Statistical comparison of survival was performed using the Mantel-Cox test. To calculate the statistical significance of the increase in SASA, a standard independent two-sample t-test was used. Statistical analyses were performed with GraphPad Prism V.7.04 software.

Additional information on the material and methods is provided in the online supplemental file.

RESULTS

We have previously reported MS-based identification of two immunogenic neoantigens ($SYTL4^{S363F}$ and $NCAPG2^{P333L}$) presented by an M_{Int} of a patient with melanoma.[7] The patient was suffering from metastatic malignant melanoma and was treated sequentially with chemotherapy and ipilimumab. Two metastases were surgically removed within a period of 24 months, resulting in complete remission. Subsequently, the patient received treatment with pembrolizumab for 1 year and has remained in sustained remission since then. Based on this case, we performed multidimensional analyses using a comprehensive material collection including a variety of tissues (B_{Lung}, M_{Lung}, M_{Int}–LN1, M_{Int}–LN2, and M_{Lung}–LN), as well as blood specimens, collected over a period of 3 years. The disease course of this patient is explained in details in the online supplemental material and shown in online supplemental figure 1).

In silico predictions complement MS-based neoantigen identification

In order to investigate whether critical neoantigens may have been missed by MS, a sequence-based prediction approach was applied. A total of 1196 missense mutations were called from M_{Int} tumor tissue, leading to prediction of ~4670 peptides (8–12 AA long) with binding affinity <500 nM. By sorting nine AA-long putative peptides according to NetMHC predicted binding affinity, previously identified neoantigens $NCAPG2^{P333L}$ and $SYTL4^{S363F}$ ranked 24th and 6th in HLA-A03:01 and HLA-B27:05 lists, respectively (online supplemental tables 1 and 2). Most peptides demonstrated also experimentally high binding affinities; however, some binding affinities partially differed from the predicted ones (online supplemental tables 1 and 2). Investigation of immunogenicity of these top-ranked nonamers binding to HLA-A03:01 and B27:05 alleles resulted in the detection of one additional confirmed neoepitope, $KIF2C^{P13L}$ (online supplemental figure 2A, B and table 1), ranking position 1 of top 25 HLA-A03:01 binding peptides according to NetMHC V.4.0 (online supplemental table 2). Molecular dynamic (MD) simulations of MHC peptide binding of $SYTL4^{S363F}$, $KIF2C^{P13L}$, and $NCAPG2^{P333L}$ were subsequently performed to elucidate differences in SASAs. Clear differences between WT and mutated peptides were observed (figure 1A–C). This was even the case for the mutated P2 of $NCAPG2^{P333L}$ harboring the mutation inside the peptide binding cleft and not at the TCR interface (figure 1C) as the larger size of the mutated residue (Leu≥Pro) shifted the position of solvent-exposed P4 Leu, increasing its SASA significantly from 108.06 Å2 (WT) to 133.54 Å2 (mutant).

In-depth characterization of immune responses against three selected neoantigens show high antigen specificity

Immune responses against $KIF2C^{P13L}$, $SYTL4^{S363F}$, and $NCAPG2^{P333L}$ neoantigens (table 1) were further analyzed in detail, and seven TCRs with specificity to these neoantigens were isolated (online supplemental table 6). SYTL4-TIL1 and SYTL4-TIL2 TCRs were isolated from TILs expanded from lung tissue after in vitro peptide stimulation and CD137-based enrichment, whereas all other TCRs were isolated from peripheral blood after in vitro stimulation and expansion as described before[7] and in the Materials and methods section. Transduction efficiency by staining of the murinized constant regions of transduced TCRs showed differences for defined TCRs, with lowest transduction rates for TCRs KIF2C-PBC1 and SYTL4-TIL2 (online supplemental figure 3). Moreover, by performing HLA class I multimer staining for all TCRs, T-cell populations binding the mutated peptide multimer could be detected only for five out of seven TCRs (online supplemental figure 4).

In vitro functional characterization of TCR-transgenic $CD8^+$ T cells showed highly specific IFN-γ secretion on recognition of target cells pulsed with mutant peptides or transduced with MGs coding for neoantigens (figure 2A–C). No reactivity was observed against WT or irrelevant peptides as well as the corresponding control MGs. Of note, transduction rates, evaluated by TCRmu staining (online supplemental figure 3), did not necessarily correlate with IFN-γ secretion as both $KIF2C^{P13L}$-specific TCRs showed similar reactivity to target LCL-1 cells presenting the mutant peptide despite major

differences in TCR expression (figure 2B). In line with that, cytokine secretion of SYTL4^{S363F}-specific TCRs was substantially higher in comparison to those reactive to KIF2C^{P13L} or NCAPG2^{P333L}, even for those TCRs with lower surface expression (figure 2A–C).

Functional avidity measurements using peptide-pulsed T2-A3 and T2-B27 cells showed EC_{50} values against respective ligands in the almost nanomolar range for all TCR-transduced T cells (figure 2D). However, TCRs specific for SYTL4^{S363F} and NCAPG2^{P333L} showed significantly higher avidities compared with KIF2C^{P13L}-specific TCRs (figure 2D, online supplemental figure 5).

To further decipher functional differences between all seven TCRs, defined cytokines as granulocyte-macrophage colony-stimulating factor (GM-CSF), IL-2, IL-12, and tumor necrosis factor alpha (TNF-α) were assessed by multiplex analysis using supernatants of TCR-transgenic CD8$^+$ T cells stimulated with mutated or WT MG-transduced LCL-1 target cells (figure 2E). Again, T cells transduced with TCRs SYTL4-TIL1 and SYTL4-PBC1 secreted the highest concentrations of these cytokines in response to respective mutated MGs.

To analyze the dynamics of TCR-mediated cytotoxic activity in vitro, an impedance-based xCELLigence system was used to monitor growth kinetics of MG transduced target cell lines after coincubation with TCR-transduced T cells. With the exception of SYTL4-PBC2, all TCRs mediated 100% lysis of MDST8^{MUT} and A2058^{MUT} target cells within 12–16 hours, while WT clones were not affected (online supplemental figure 6A–C). Among SYTL4^{S363F}-specific TCRs, SYTL4-TIL1 showed the fastest rejection dynamics (online supplemental figure 6A). With respect to KIF2C^{P13L}-specific TCRs, rejection dynamics again appear to be similar despite different transduction rates (online supplemental figure 6B). Comparison of cytotoxic potential for all TCRs showed different dynamics dependent on the target cells but comparable final effects except for SYTL4-PBC2 displaying an inferior cytolysis pattern (online supplemental figure 6D).

TCRs show neoantigen-specific binding and low cross-reactivity patterns

A set of altered peptide ligands containing individual alanine or threonine replacements (ala/thr scan) at every single position of the cognate neoantigen was used to investigate the cross-reactivity potential of defined TCR-transgenic T cells (figure 3). Highly similar recognition patterns of all four SYTL4^{S363F}-specific TCRs were observed despite highly diverse TCR sequences (figure 3A and online supplemental table 7). These results suggest a similar peptide–HLA docking pattern for all TCRs with this neoantigen specificity. In contrast, recognition patterns of exchange ala/thr motifs were slightly more variable with respect to both KIF2C^{P13L}-specific TCRs (figure 3B). This was reflected by a higher potential for cross-reactivity against naturally occurring peptides within the human proteome, as investigated by ScanProsite tool (https://prosite.expasy.org/

Table 1 Characteristics of neoantigens targeted by identified TCRs

Peptide name	Gene name	Ensembl transcript ID	Peptide sequence	HLA restriction	Predicted affinity (nM), rank (%)	Experimental IC_{50} (nM)	MS FDR (%)	Reads exome PBMCs (Ref:Alt)	Reads exome M_{int} (Ref:Alt)	Reads exome M_{Lung} (Ref:Alt)
SYTL4^{S363F}	SYTL4	ENST00000263033	GRIAF**F**LKY	B27:05	18.43; 0.6	214.7±1.8	1	54:0	32:10	71:20
SYTL4^{WT}			GRIAF**S**LKY		30.62; 0.12	97.32±2.1				
KIF2C^{P13L}	KIF2C	ENST00000372224	RLF**L**GLAIK	A03:01	21.6; 0.09	237.4±2.0		75:0	75:18	177:21
KIF2C^{WT}			RLF**P**GLAIK		12.10; 0.03	146.2±1.1				
NCAPG2^{P333L}	NCAPG2	ENST00000409339	K**L**ILWRGLK	A03:01	32.6; 0.15	202.9±1.03	1	126:0	146:27	54:0
NCAPG2^{WT}			K**P**ILWRGLK		6946.48; 6.50	4,488.7±10.4				

Alt, alternative read; FDR, false discovery rate; HLA, human leukocyte antigen; IC_{50}, half maximal inhibitory concentration; M_{int}, intestinal metastasis; M_{Lung}, lung metastasis; PBMC, peripheral blood mononuclear cell; Ref, reference read; TCR, T-cell receptor.

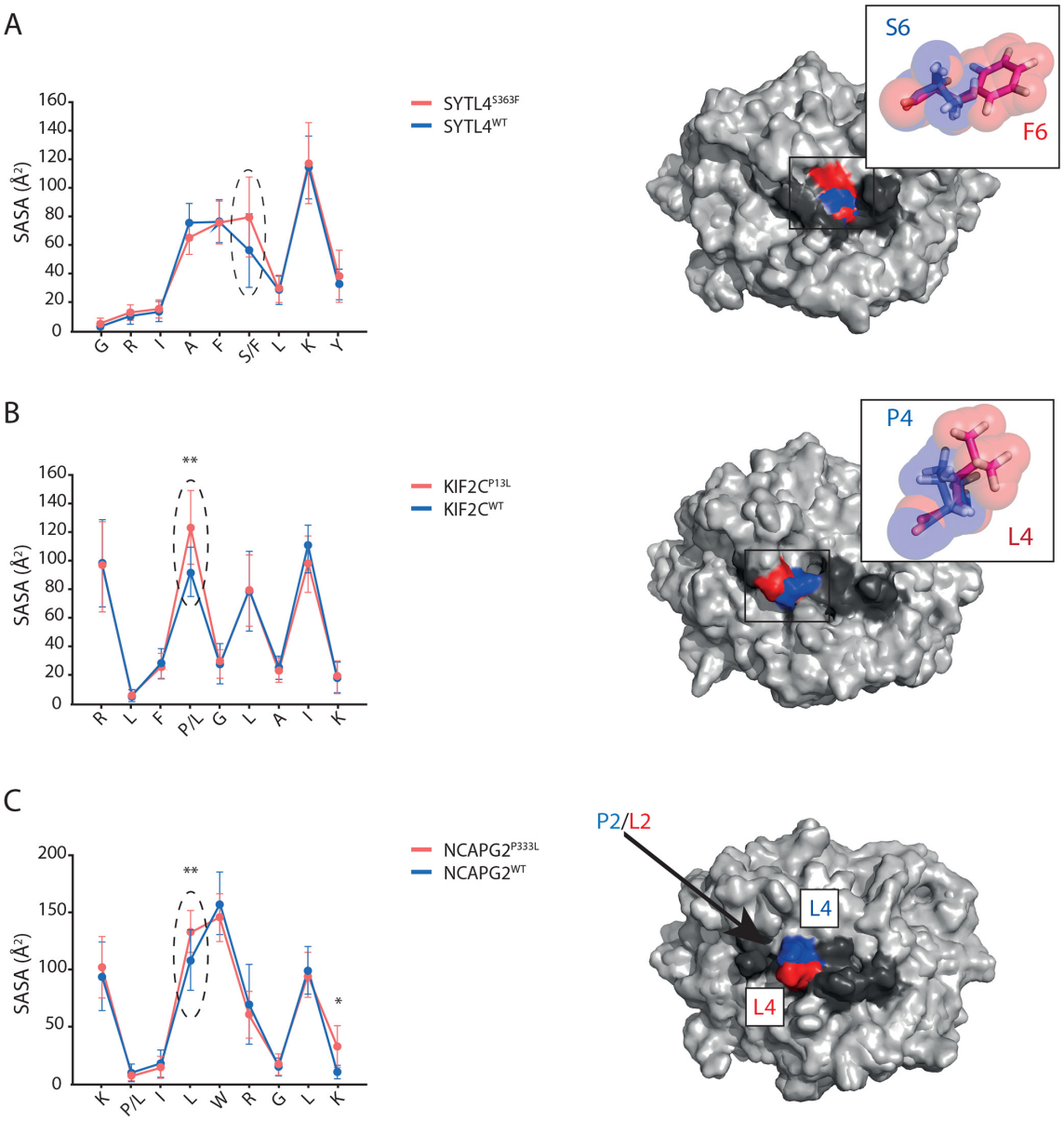

Figure 1 Mutations result in distinct antigen features as shown by structural modeling. (A–C) Residue-specific SASA values of the neoantigen (red) and its respective WT (blue) are plotted on the left side. Corresponding superimposed representative structures as extracted from MD simulations are shown on the right side for SYTL4^{S363F} (A), KIF2C^{P13L} (B), and NCAPG2^{P333L} (C). HLA peptide complexes (right side) are shown in surface representation with HLA (light gray), peptide (dark gray) and central positions of increased SASA in red (neoantigen) and blue (WT). Latter positions are emphasized in the SASA plots by black arrows and dashed line ellipses. (A,B) Mutated residues are depicted in sticks and transparent spheres to illustrate physicochemical differences. (C) The arrow indicates the buried mutation site. SASA mean value and SD of each individual peptide AA were calculated out of three replicates. *P<0.05, **P<0.01. HLA, human leukocyte antigen; MD, molecular dynamic; SASA, solvent-accessible surface area; WT, wild type.

scanprosite).[17] SYTL4^{S363F}-specific and NCAPG2^{P333L}-specific TCRs exhibited potential cross-reactivity with four to six antigens only, while KIF2C^{P13L}-specific TCRs might recognize >400 targets (online supplemental table 7). The potential discrepancy in cross-reactivity was tested in vitro with a selection of the ScanProsite retrieved peptides according to predicted binding affinity to HLA-A03:01 and B27:05 (online supplemental table 8). This small-scale screening did not show any reactivity of the TCRs against the selected peptides (online supplemental figure 7). Moreover, the alloreactive potential of selected TCRs tested against a panel of LCLs expressing the most frequent HLA allotypes (online supplemental table 5) with or without previous peptide pulsing showed low alloreactive potential for all neoantigen-specific TCRs (online supplemental figure 8).

Neoantigen-specific TCRs display in vivo antitumor potential

We next asked whether differences of in vitro functionality, especially with respect to SYTL4^{S363F}-specific and KIF2C^{P13L}-specific TCRs, may also lead to different in vivo tumor rejection patterns (figure 4). Therefore, antitumor

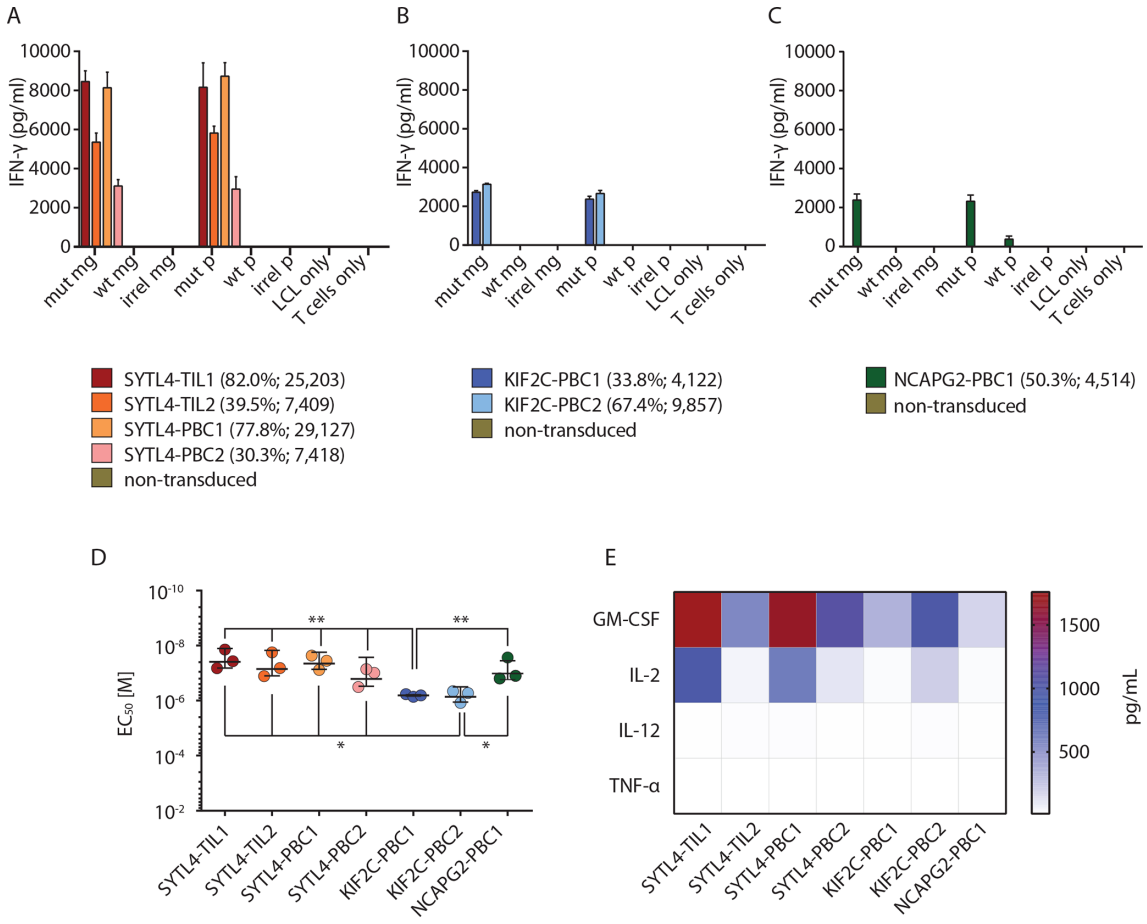

Figure 2 High specificity and strong functional performance of identified TCRs in vitro. (A–C) Secretion of IFN-γ by CD8$^+$ T cells transduced with TCRs specific for SYTL4^{S363F} (A), KIF2C^{P13L} (B), and NCAPG2^{P333L} (C) after coculture with LCL-1-presenting neoantigens and respective WT counterparts at effector to target (E:T)=1:1 is shown. LCL-1 transduced with MGs encoding for fragments of mut sequence (mut MG), WT sequence (WT MG) or irrelevant sequence (irrel MG) were compared with peptide pulsed LCLs (mut P, WT P, irrel P; 1 µM peptide). IFN-γ secretion in supernatants was investigated by ELISA assay. Bars represent average reads from three duplicates; error bars represent SD transduction efficiencies; and Mean Fluorescent Intensity (MFI) values are indicated below the graphs. (D) Comparison of functional avidity of neoantigen-specific TCRs, calculated as EC_{50} of cognate mutated peptide. IFN-γ secretion was assessed on supernatants, and a non-linear curve was fit to determine the EC_{50} value. EC_{50} values deriving from three different experiments were depicted for each TCR. Bars in the graph represent the mean value, and SD significance is calculated with one-way analysis of variance and Tukey multiple comparison test (*p≤0.05, **p≤0.01). (E) Assessment of multicytokine secretion of TCR-transduced T cells on coculture with LCL-1 pulsed with mutated peptides. All experiments were performed at least with three different sets of transduced T cells derived from two different healthy donors. EC_{50}, half maximal effective concentration; IFN, interferon; LCL, lymphoblastoid cell line; MG, minigene; mut, mutant; TCR, T-cell receptor; WT, wild type.

reactivity of defined neoantigen-specific TCRs was investigated in a xenograft murine model using a MG-transduced U-698-M lymphoma model. U-698-M tumor growth in NSG mice was monitored starting from 5 days before intravenous T-cell injection. TCR-transduced T cells were normalized to approximately 62%, except for KIF2C-PBC1, for which transduction rate was about 14% (online supplemental table 9). Around day 4 post-T-cell injection, tumors of mice that received T cells expressing a control TCR kept constantly growing, while tumors in hosts receiving T cells transduced with TCRs SYTL4-TIL1, SYTL4-PBC1, KIF2C-PBC1, and KIF2C-PBC2 completely rejected the tumor (figure 4A). Of note, tumor rejection by T cells transduced with KIF2C-PBC2 and especially KIF2C-PBC1 with lower transduction rate showed very good rejection kinetics. Survival curves visualize that mice injected with control TCR 2.5D6 developed uncontrolled tumor growth with ulcerations beginning at day 10 and subsequently had to be euthanized, whereas neoantigen-specific TCRs mediated significantly prolonged survival (figure 4B). Flow cytometry data show infiltration of mutated tumors by respective TCRs at day 4 after first T-cell injection (online supplemental figure 9) as well as persistence of TCR-transgenic T cells in the spleen, bone marrow and blood at day 20 (figure 4C). Observed frequencies of TCRmu$^+$ T cells among all CD8$^+$ lymphocytes in these compartments reflect frequencies of transferred TCR-transgenic T cells.

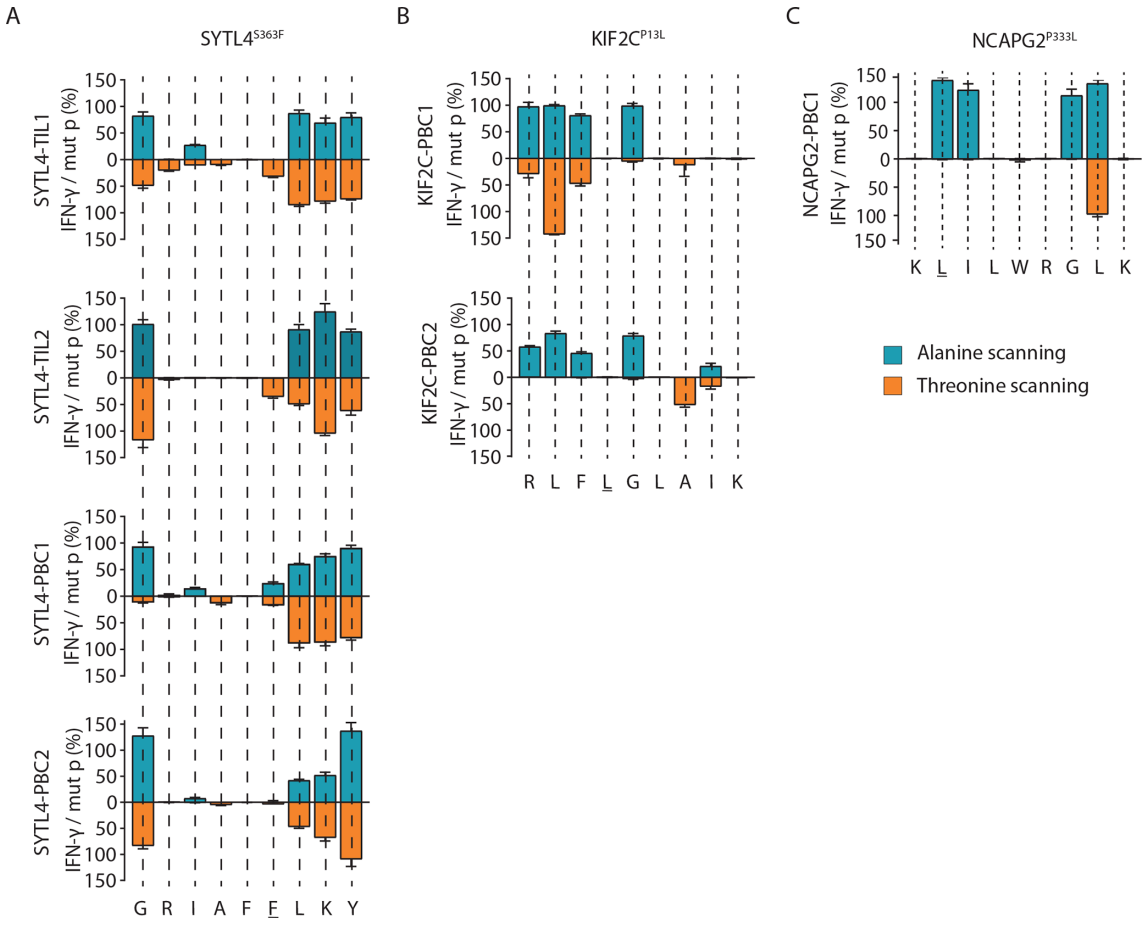

Figure 3 Cross-reactivity analyses indicate antigen-dependent TCR docking on HLA peptide complexes. (A–C) TCR cross-reactivity was tested by quantification of secreted IFN-γ on coculturing TCR-transduced T cells with T2 target cells pulsed with ala/thr scanned peptide cognates (1 µM peptide) of ligands SYTL4^{S363F} (A), KIF2C^{P13L} (B), and NCAPG2^{P333L} (C). IFN-γ secretion values from single conditions were normalized against the cytokine level in response to the defined neoantigen. HLA, human leukocyte antigen; IFN, interferon; TCR, T-cell receptor.

Antigen-dependent spatial and temporal distribution of identified TCRs in blood and tissues

To investigate spatial and temporal distributions of tumor antigen-specific TCR clonotypes within the patient's tissues and blood, TCR-β deep sequencing was performed by extracting gDNA from B_{Lung}, M_{Int}, M_{Lung}, LNs, as well as PBMCs from different time points (online supplemental figure 1).

Overlap of TCR-β clonotypes was investigated in all three tumor tissues. All tumor samples, resected over a time span of 8 years, share 29 TCR-derived CDR3 (online supplemental figure 10A). M_{Int} and M_{Lung}, closer in time, share 3072 TCR clonotypes (14.77% of all sequences identified in M_{Int} and M_{Lung}). Notably, a number of 462 TCR clonotypes were shared between both resected metastases and all analyzed adjacent LNs (online supplemental figure 10B).

The seven characterized neoantigen-specific TCRs were tracked within metastasized tumor lesions, LNs and blood samples (figure 5 and online supplemental figure 8). Frequencies of these TCRs identified from peripheral blood specimens, LNs and tumor tissue are shown in online supplemental tables 10 and 11). KIF2C^{P13L}-specific TCRs were the most abundant in all metastasized tumor tissues over time, and TCR KIF2C-PBC1 could be detected in B_{Lung} even prior to therapy with Ipilimumab. Overall, frequency of KIF2C^{P13L}-specific TCRs, especially KIF2C-PBC2, was increasing in M_{Lung} compared with M_{Int} (figure 5A and online supplemental table 10), whereas frequencies of SYTL4^{S363F}-specific TCRs were decreasing or remained stable. Notably, TCR NCAPG2-PBC1 could not be detected in M_{Lung}, corresponding to the lack of detectability of this specific mutation in the metastasis on the exome level (figure 5A and table 1). By investigating the relative frequency of known neoantigen-specific TCRs among all identified CDR3 sequences in tumor-associated non-malignant LNs, the overall percentage of all seven cognate TCRs contributing to the analyzed TCR repertoire was calculated, ranging from 0.11% to 1.53% (figure 5B). Thereby, TCRs specific for KIF2C^{P13L} comprised the highest relative percentage not only in tumor tissues but also in tumor-associated LNs. However, we observed relative frequency of defined TCR clonotypes being more evenly distributed in associated LNs (figure 5B).

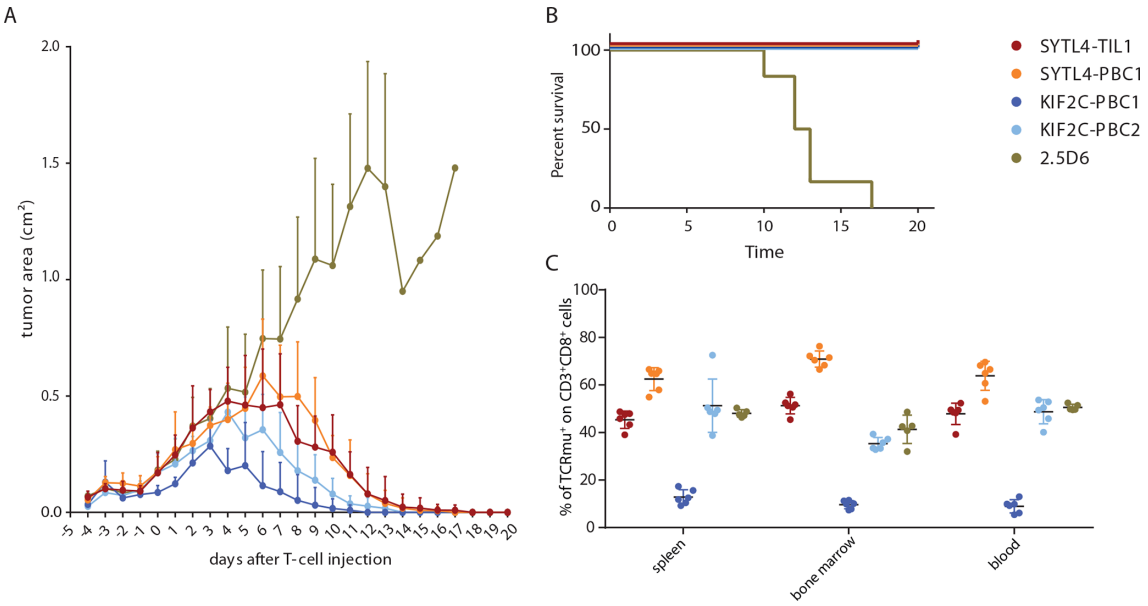

Figure 4 Performance of T cells transgenic for neoantigen-specific TCRs in vivo. (A) Growth kinetics of U-698-M tumors expressing neoantigens (area in mm^2) in NSG mice. Mean values and SDs are depicted for each group of mice to monitor rejection dynamics (n=6). Animals were intravenously injected with a total of 2×10^7 T cells on day 0+1. Tumor growth was significantly impaired in all mice receiving neoantigen-specific TCRs in comparison to 2.5D6 at day 10 (adjusted p value of 0.0001, calculated with two-way analysis of variance (time and treatment) and multiple comparison Dunnett's test). (B) Kaplan-Meier survival curve of tumor-bearing mice injected with different TCR-transduced T cells. Survival of animals receiving neoantigen-specific TCRs was significantly prolonged to 2.5D6 (p<0.0001, Mantel-Cox test) (C), percentage of $TCRmu^+$ T cells among all infiltrating $CD3^+CD8^+$ T cells in spleen, bone marrow and blood. Organs of animals receiving 2.5D6-transgenic T cells were processed at the respective day of removal. One control mouse receiving 2.5D6-transgenic T cells did not exhibit a clear population of infiltrating T cells and was therefore excluded from this analysis. All other animals with transferred neoantigen-specific TCR constructs were analyzed at day 20 exhibiting complete tumor rejection. TCR, T-cell receptor.

In peripheral blood, all specific TCRs could be detected in at least four out of the six sequenced samples (figure 5C). Productive frequencies of $SYTL4^{S363F}$-specific TCRs ranged between 0.0008% to maximal 0.013%, whereas TCRs KIF2C-PBC1, KIF2C-PBC2, and NCAPG2-PBC1 showed considerably higher frequencies between 0.013% and 0.54% in analyzed blood samples (online supplemental table 11). Of note, TCR KIF2C-PBC1 showed again the highest frequencies over time. In contrast, frequency of TCR KIF2C-PBC2 in peripheral blood increases up to the time point of resection of the M_{Lung} and decreases thereafter corresponding to the high frequency of this TCR in M_{Lung} and associated LN (figure 5C).

Presence of identified TCR KIF2C-PBC2 within respective primary tumor tissue was verified additionally by TCR imaging using RNA hybridization BaseScope assay on tumor M_{Lung} (online supplemental figure 11). In addition, mutated ligand $KIF2C^{P13L}$ was also recognized by isolated TILs of the patient (online supplemental figure 12).

T cells specific for $SYTL4^{S363F}$ and $KIF2C^{P13L}$ display divergent activation profiles

To further delineate TCR-dependent differences, we aimed to investigate activation parameters of neoantigen-specific stimulated T cells. We exemplarily explored expression of the T-box transcription factor TBX21 (T-bet) and programmed cell death protein 1 (PD-1) expression on SYLT4-TIL1, -PBC1, KIF2C-PBC1, and KIF2C–PBC2 transduced T cells after coculture with MG-transduced U-698-M. $SYTL4^{S363F}$-specific TCR displayed a higher upregulation of T-bet after 24 hours compared with $KIF2C^{P13L}$-specific constructs with all TCR showing a downregulation of expression to baseline after 96 hours (online supplemental figure 13A–B). To minimize the potential influence of different transduction rates, T cells transduced with TCRs SYTL4-TIL1 and KIF2C-PBC2 were enriched using near -infrared fluorescent protein (iRFP)-containing constructs. Using enriched populations, we observed marked differences of IFN-γ secretion between TCRs with defined specificities on antigen-specific stimulation (figure 6A), as shown for non-enriched transduced T cells (figure 2A,B). Investigating early T-cell activation, we observed a higher upregulation of T-bet for SYTL4-TIL1-iRFP after 24 hours compared with KIF2C-PBC2-iRFP (figure 6B,C, and online supplemental figure 13C–D). Also, upregulation of PD-1 was higher after 24 hours in SYTL4-redirected T cells in comparison to KIF2C-PBC2 with respect to frequency and MFI of $PD\text{-}1^+$ T cells (figure 6D,E). Yet, in vitro rechallenging of neoantigen-specific T cells after 11 days contrarily revealed an almost equal IFN-γ secretion of both TCRs on stimulation with U-698-M expressing the mutated MG (figure 6F). In this regard, T-bet and PD-1 expression of KIF2C-PBC2-iRFP was at the same level as SYTL4-TIL1-iRFP (figure 6G–J).

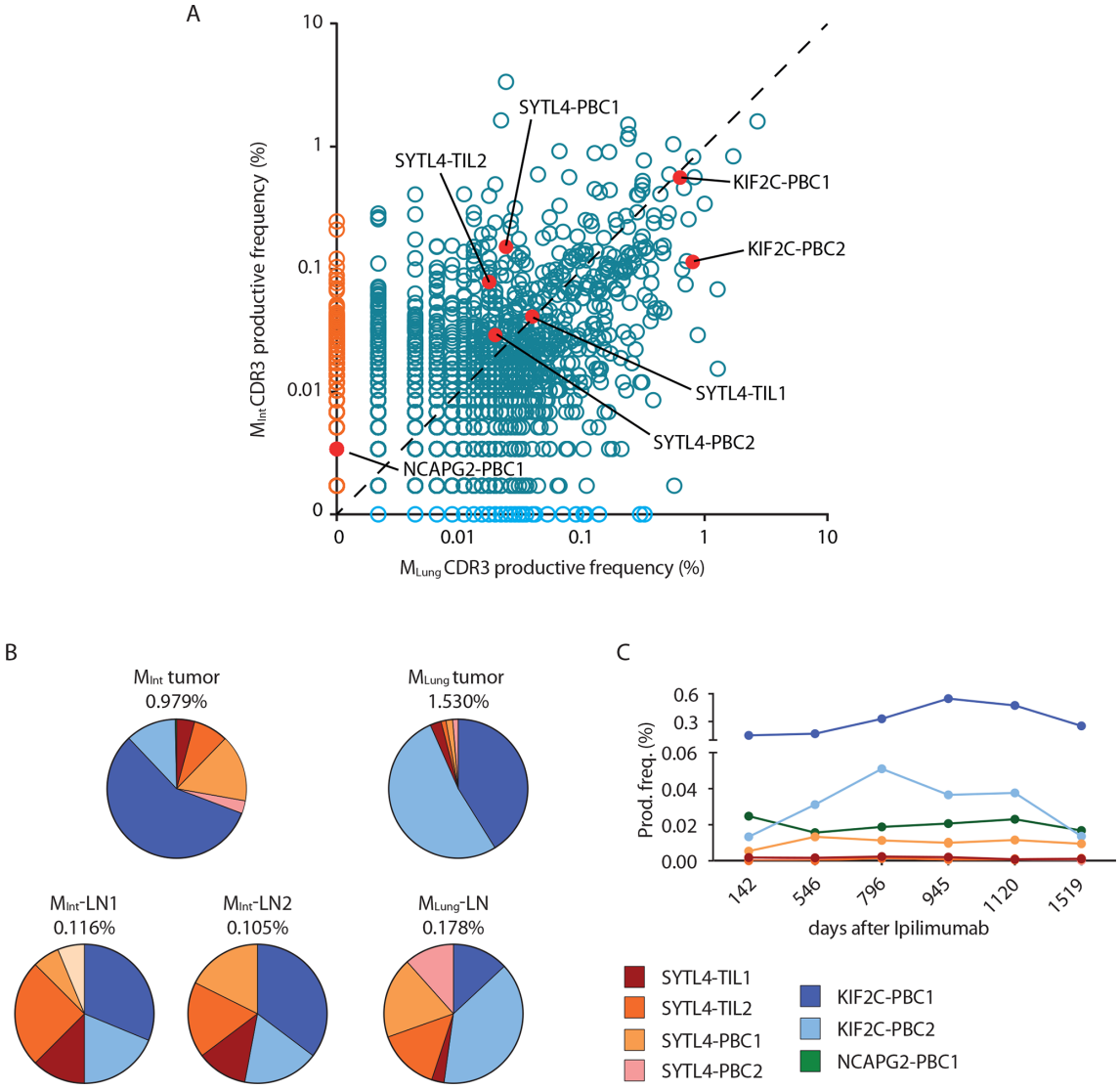

Figure 5 Spatial and temporal distribution of neoantigen-specific TCRs as determined by TCR-β sequencing. (A) Productive frequency of CDR3 rearrangements (amino acid) calculated as the number of sequencing templates divided by the sum of template counts for all productive rearrangements in M_{Int} and M_{Lung}. Scatter plot dataset was generated with adaptive Biotechnologies ImmunoSEQ analysis software. (B) Distribution of neoantigen-specific TCRs in resected tumor and lymph node tissues. Percentages indicate frequency of identified neoantigen-specific TCRs in analyzed tissue repertoire as inferred from TCR-β deep sequencing data. (C) Productive frequency expressed as percentage of neoantigen-specific clonotypes in peripheral blood at different time points after first treatment with ipilimumab. TCR, T-cell receptor.

DISCUSSION

Within this study, we performed an in-depth characterization of TCR specifically recognizing neoantigens derived from somatic mutations which have been identified in malignant tissue of a patient with melanoma. We thereby reveal important insights with potential relevance for the development of advanced personalized immunotherapies targeting neoantigens.

For neoantigen identification, MS-based immunopeptidomics and in silico peptide prediction were applied using a patient-specific database of SNVs. SYTL4^{S363F} and NCAPG2^{P333L} neoantigens have been detected by MS as previously reported,[7] whereas KIF2C^{P13L} has been primarily identified through in silico prediction of high-affinity HLA binders. However, this peptide could be meanwhile detected by MS using novel machine learning algorithms demonstrating the power of this approach.[18] Experimental affinity measurements of selected predicted peptides showed similar IC_{50} values for all three neoantigens, although no real correlation to predicted affinity was observed for the whole cohort of analyzed peptides. Furthermore, experimental and in silico determined affinity are not accurate immunogenicity predictors in our case. MDs confirmed previous reports pointing to the fact that antigen recognition may depend not only on a defined mutation but also on conformational changes affecting the adjacent AAs.[19] Moreover, our data confirm that structural parameters as SASA can be used to improve prediction of suitable neoantigens and may be a valuable addition to comprehensive neoantigen selection algorithms.[20]

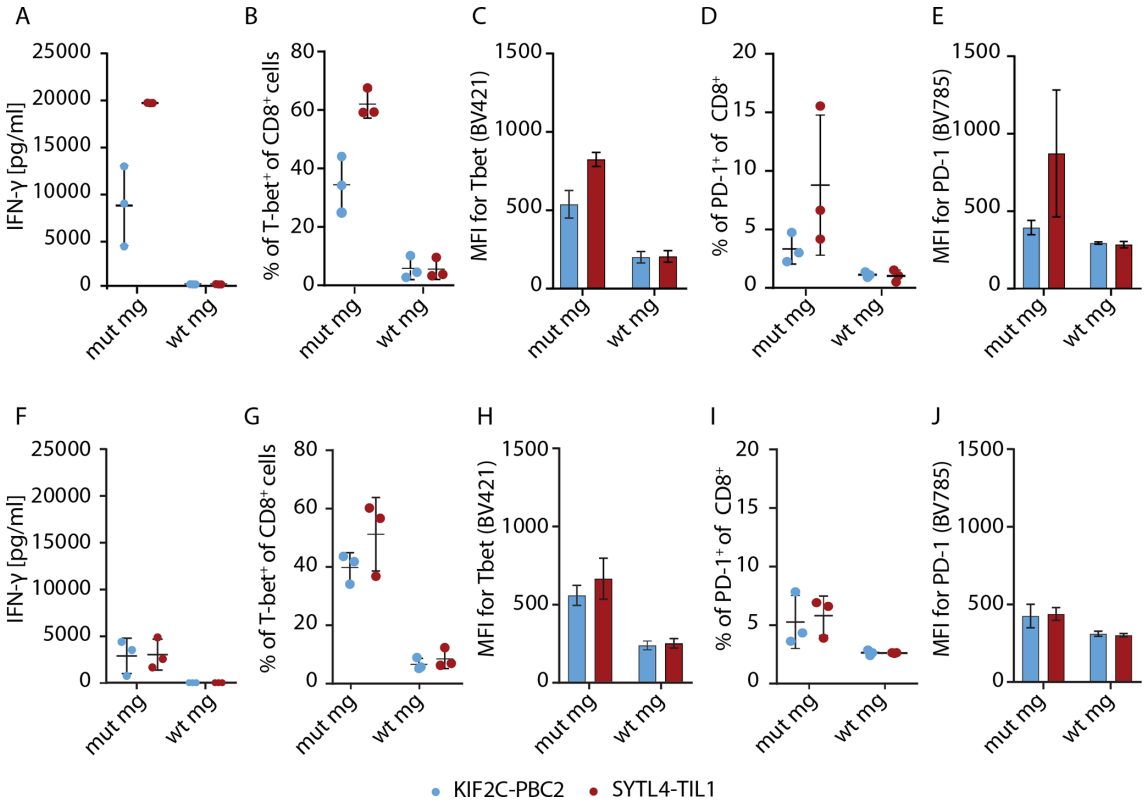

Figure 6 T-cell activation and dysfunction of enriched SYTL4-TIL1-iRFP and KIF2C-PBC1-iRFP TCR on neoantigen stimulation with MG-transduced U-698-M. (A) IFN-γ secretion of T cells 24 hours after coculture. (B–E) Expression of specific markers 24 hours after coculture: percentage of T-bet$^+$ cells within CD8$^+$ T cells (B), MFI for T-bet of CD8$^+$ T cells (C), percentage of PD-1$^+$ cells within CD8$^+$ T cells (D) and MFI for PD-1 of CD8$^+$ T cells (E). (F,J) T-cell activation and dysfunction was comparably assessed 24 hours after second stimulation of SYLT4-TIL1-iRFP and KIF2C-PBC2-iRFP transgenic T cells with MG-expressing target cells at day 11 after initial stimulation. Results of transduced T cells from three different donors are shown. MG, minigene; PD-1, programmed cell death protein 1; TCR, T-cell receptor.

Interestingly, the somatic mutation coding for KIF2C^{P13L} peptide is in close proximity to another one previously reported. The latter results in an immunogenic decamer which overlaps our neoantigen by eight AAs.[21] This finding may further support the notion of existing hotspots for peptide presentation and emphasizes that genes especially activated in cancer, such KIF2C, may preferentially result in peptide ligands.[22]

Although several groups have published data describing neoantigen-specific TCRs,[23–26] the data shown here provide a much deeper insight. We observed oligoclonal endogenous T-cell responses against two antigens within one patient. We showed recognition of endogenously processed neoantigens as well as tumor reactivity in vitro and in vivo by all identified TCRs. Of particular interest, TCRs with identical specificity showed similar characteristics with regard to temporal and spatial distribution in the body, functional avidity, functionality, and docking pattern as investigated by alanine/threonine scans, suggesting a major role of the antigen or MHC-peptide docking by the TCR driving defined immune responses. Functional avidities of all seven TCRs were in a narrow range, yet TCRs with specificity for KIF2C^{P13L} showed significant lower avidities compared with the other receptors and a much higher frequency in both metastatic lesions, adjacent LNs as well as the peripheral blood over time. Moreover, despite inferior cytokine secretion in relation to SYTL4^{S363F}-specific TCRs in vitro, both KIF2C^{P13L}-specific TCRs demonstrated especially effective tumor rejection potential, with KIF2C-PBC1 showing even a markedly lower transduction rate. We suggest that highly activated TCRs may be more prone to T-cell dysfunction[27 28] as previously demonstrated for CAR-T cells.[29] This hypothesis is further corroborated by high PD-L1 expression on patients' tumor cells within M_{Lung} [7] potentially inducing a PD-L1-mediated dysfunctional state. In vitro data of TCR-transgenic T cells suggest a different activation signature exemplarily tested for SYTL4-TIL1 in comparison to KIF2C-PBC2, with SYTL4-TIL1 displaying a higher PD-1 and an elevated T-bet expression on neoantigen-specific stimulation. Differences in T-bet upregulation may be associated to skewing CD8$^+$ T cells towards a short-lived effector phenotype and may contribute to a dysfunctional state.[30 31] Interestingly, levels of IFN-γ secretion, T-bet and PD-1 expression substantially decreased on restimulation of highly activated SYTL4-TIL1 in contrast to KIF2C-PBC2. These data may indicate a disadvantage of SYTL4-specific T cells with respect to sustained function. Our data therefore suggest that future engineering of TCR and respective transgenic T cells may be considered

as a very personalized task for the individual TCR. This may affect defined comprehensive T-cell engineering measures as PD-1 knock-down as well as affinity maturation of tumor-specific TCRs.[32–34] Yet, further investigations implementing multiparametric transcriptional profiling are needed for a deeper understanding and dissection. Advantages of TCRs with lower avidity with respect to persistence have been recently reported for virus-specific T cells,[35] and the observations might coincide with maintenance of such TCRs throughout presentation of similar peptides, potentially leading to cross-reactive stimulation.[36] Interestingly, occurrence of side effects correlates with favorable clinical response in patients treated with immune checkpoint inhibitors, suggesting that cross-reactivity may in fact be to some extent beneficial.[37] Despite this, no major side effects associated with ipilimumab were observed in the clinical history of the patient and no cross-reactivity was observed in vitro for investigated peptides. In the case of NCAPG2^{P333L}, the coding mutation was lost during progression of disease, coinciding with low frequencies of this TCR and loss of detection of this clonotype in M_{Lung}. However, despite low frequencies, both SYTL4^{S363F}-specific and NCAPG2^{P333L}-specific TCRs could be still isolated from peripheral blood or TILs, indicating the presence of non-terminally exhausted memory T cells with potential for expansion. Moreover, non-malignant LNs may also represent an attractive source for isolation of such neoantigen-specific TCRs.

In retrospect, we have identified seven endogenous neoantigen-specific TCRs with high potential for transgenic modification of T cells, to be used for adoptive T-cell transfer. Our data provide evidence that TCRs display different qualities in vitro and in vivo, which seem to be TCR class dependent and need to be taken into account in the context of adoptive T-cell transfer of neoantigen-specific TCR-transgenic T cells.

Author affiliations
[1]Klinik und Poliklinik für Innere Medizin III, Klinikum rechts der Isar der Technischen Universität München, München, Germany
[2]Laboratory of Protein Biochemistry, Institute for Chemistry and Biochemistry, Freie Universität Berlin, Berlin, Germany
[3]Institute of Molecular Oncology and Functional Genomics, TUM School of Medicine, Klinikum rechts der Isar der Technischen Universität München, München, Germany
[4]Center for Translational Cancer Research (TranslaTUM), TUM School of Medicine, Klinikum rechts der Isar der Technischen Universität München, München, Germany
[5]TUM School of Life Sciences and Center for Integrated Protein Science Munich, Klinikum rechts der Isar der Technischen Universität München, München, Germany
[6]Department of Medicine II, Klinikum rechts der Isar, TUM School of Medicine, Klinikum rechts der Isar der Technischen Universität München, München, Germany
[7]Institute for Medical Microbiology Immunology and Hygiene, Technische Universität München, München, Germany
[8]Institute of Pathology, School of Medicine, Klinikum rechts der Isar der Technischen Universität München, München, Germany
[9]MRI-TUM-Biobank at the Institute of Pathology, School of Medicine, Klinikum rechts der Isar der Technischen Universität München, München, Germany
[10]Core Facility Experimental Pathology, School of Medicine, Klinikum rechts der Isar der Technischen Universität München, München, Germany
[11]German Cancer Consortium (DKTK), partner-site Munich, and German Cancer Research Center (DKFZ) Heidelberg, Heidelberg, Germany

Acknowledgements The authors thank the patient for participating in the study and his continuous support. We also thank Anja Stelzl for excellent technical support as well as Jürgen Schlegel and Sandra Baur (TU München, Department of Neuropathology, Munich, Germany) for technical advice.

Contributors EB, GL, and AK designed the study. EB, GL, ETA, DG, FF, HL, SA, ME, YC, KY, and CA conducted and analyzed experiments. NdAK, LW, SL, and TE performed bioinformatics. EB, GL, FF, MB, and KS validated data. FB, WW, DHB, RR, CF, IA, and AK acquired funding and provided resources. WW, DHB, RR, CF, IA, and AK supervised the project or parts of it. EB, GL, NdAK, LW, and AK wrote the manuscript. All authors reviewed and edited the manuscript.

Funding This work was supported by grants to AMK from EIT Health (number 19638), Deutsche Krebshilfe (110281) and Wilhelm Sander-Stiftung (2015.030.1), as well as to AMK and IA from Deutsche Forschungsgemeinschaft (SFB824/C10, TRR338, SFB1035/A10 and CIPSM) and the Technical University of Munich and International Graduate School of Science and Engineering.

Competing interests No, there are no competing interests.

Patient consent for publication Not required.

Ethics approval Informed consent of all healthy donors and the patient was obtained following requirements of the institutional review board (Ethics Commission, Faculty of Medicine, TUM) and in accordance with the principles of the Declaration of Helsinki

Provenance and peer review Not commissioned; externally peer reviewed.

Data availability statement Data are available upon reasonable request. All data relevant to the study are included in the article or uploaded as supplementary information.

ORCID iDs
Eva Bräunlein http://orcid.org/0000-0001-9640-3741
Franziska Füchsl http://orcid.org/0000-0001-5069-1442
Dario Gosmann http://orcid.org/0000-0002-4973-4801
Sebastian Lange http://orcid.org/0000-0003-0406-1401
Thomas Engleitner http://orcid.org/0000-0002-7989-681X
Melanie Boxberg http://orcid.org/0000-0001-5989-7922
Katja Steiger http://orcid.org/0000-0002-7269-5433
Florian Bassermann http://orcid.org/0000-0003-4435-2609
Wilko Weichert http://orcid.org/0000-0001-6139-8372
Dirk H Busch http://orcid.org/0000-0001-8713-093X
Roland Rad http://orcid.org/0000-0002-6849-9659
Christian Freund http://orcid.org/0000-0001-7416-8226
Iris Antes http://orcid.org/0000-0002-2241-7187
Angela M Krackhardt http://orcid.org/0000-0002-4752-0543

REFERENCES

1 Topalian SL, Drake CG, Pardoll DM. Immune checkpoint blockade: a common denominator approach to cancer therapy. *Cancer Cell* 2015;27:450–61.
2 Samstein RM, Lee C-H, Shoushtari AN, *et al*. Tumor mutational load predicts survival after immunotherapy across multiple cancer types. *Nat Genet* 2019;51:202–6.
3 Ott PA, Hu Z, Keskin DB, *et al*. An immunogenic personal neoantigen vaccine for patients with melanoma. *Nature* 2017;547:217–21.

4 Sahin U, Derhovanessian E, Miller M, *et al*. Personalized RNA mutanome vaccines mobilize poly-specific therapeutic immunity against cancer. *Nature* 2017;547:222–6.
5 Tran E, Robbins PF, Lu Y-C, *et al*. T-Cell transfer therapy targeting mutant KRAS in cancer. *N Engl J Med* 2016;375:2255–62.
6 Kalaora S, Wolf Y, Feferman T, *et al*. Combined analysis of antigen presentation and T-cell recognition reveals restricted immune responses in melanoma. *Cancer Discov* 2018;8:1366–75.
7 Bassani-Sternberg M, Bräunlein E, Klar R, *et al*. Direct identification of clinically relevant neoepitopes presented on native human melanoma tissue by mass spectrometry. *Nat Commun* 2016;7:13404.
8 Wang X, Berger C, Wong CW, *et al*. Engraftment of human central memory-derived effector CD8+ T cells in immunodeficient mice. *Blood* 2011;117:1888–98.
9 McMahon RM, Friis L, Siebold C, *et al*. Structure of HLA-A*0301 in complex with a peptide of proteolipid protein: insights into the role of HLA-A alleles in susceptibility to multiple sclerosis. *Acta Crystallogr D Biol Crystallogr* 2011;67:447–54.
10 Hülsmeyer M, Welfle K, Pöhlmann T, *et al*. Thermodynamic and structural equivalence of two HLA-B27 subtypes complexed with a self-peptide. *J Mol Biol* 2005;346:1367–79.
11 Hartmann C, Antes I, Lengauer T. IRECS: a new algorithm for the selection of most probable ensembles of side-chain conformations in protein models. *Protein Science* 2007;16:1294–307.
12 Humphrey W, Dalke A, Schulten K. VMD: visual molecular dynamics. *J Mol Graph* 1996;14:33–8.
13 Varshney A, Brooks JF, William J. Linearly scalable computation of smooth molecular surfaces. *IEEE Comp Graph Appl* 1997;14 https://www.cs.umd.edu/~varshney/papers/av_cga.pdf
14 Klar R, Schober S, Rami M, *et al*. Therapeutic targeting of naturally presented myeloperoxidase-derived HLA peptide ligands on myeloid leukemia cells by TCR-transgenic T cells. *Leukemia* 2014;28:2355–66.
15 Audehm S, Glaser M, Pecoraro M, *et al*. Key features relevant to select antigens and TCR from the MHC-mismatched repertoire to treat cancer. *Front Immunol* 2019;10:1485.
16 Mall S, Yusufi N, Wagner R, *et al*. Immuno-PET imaging of engineered human T cells in tumors. *Cancer Res* 2016;76:4113–23.
17 de Castro E, Sigrist CJA, Gattiker A, *et al*. ScanProsite: detection of PROSITE signature matches and prorule-associated functional and structural residues in proteins. *Nucleic Acids Res* 2006;34:W362–5.
18 Wilhelm M, Zolg DP, Graber M, *et al*. Deep learning boosts sensitivity of mass spectrometry-based immunopeptidomics. *Nat Commun* 2021;12:3346.
19 Ebrahimi-Nik H, Michaux J, Corwin WL, *et al*. Mass spectrometry–driven exploration reveals nuances of neoepitope-driven tumor rejection. *JCI Insight* 2019;4.
20 Zaidi N, Soban M, Chen F, *et al*. Role of in silico structural modeling in predicting immunogenic neoepitopes for cancer vaccine development. *JCI Insight* 2020;5.
21 Lu Y-C, Yao X, Crystal JS, *et al*. Efficient identification of mutated cancer antigens recognized by T cells associated with durable tumor regressions. *Clin Cancer Res* 2014;20:3401–10.
22 Caron E, Vincent K, Fortier Marie-Hélène, Fortier MH, *et al*. The MHC I immunopeptidome conveys to the cell surface an integrative view of cellular regulation. *Mol Syst Biol* 2011;7:533.
23 Tran E, Ahmadzadeh M, Lu Y-C, *et al*. Immunogenicity of somatic mutations in human gastrointestinal cancers. *Science* 2015;350:1387–90.
24 Chheda ZS, Kohanbash G, Okada K, *et al*. Novel and shared neoantigen derived from histone 3 variant H3.3K27M mutation for glioma T cell therapy. *J Exp Med* 2018;215:141–57.
25 Matsuda T, Leisegang M, Park J-H, *et al*. Induction of neoantigen-specific cytotoxic T cells and construction of T-cell receptor–engineered T cells for ovarian cancer. *Clin Cancer Res* 2018;24:5357–67.
26 Ren L, Leisegang M, Deng B, *et al*. Identification of neoantigen-specific T cells and their targets: implications for immunotherapy of head and neck squamous cell carcinoma. *Oncoimmunology* 2019;8:e1568813.
27 Alexander-Miller MA, Leggatt GR, Sarin A, *et al*. Role of antigen, CD8, and cytotoxic T lymphocyte (CTL) avidity in high dose antigen induction of apoptosis of effector CTL. *J Exp Med* 1996;184:485–92.
28 Santa SD, Merlo A, Bobisse S, *et al*. Functional avidity–driven activation-induced cell death shapes CTL immunodominance. *J Immunol* 2014;193:4704–11.
29 Chmielewski M, Hombach A, Heuser C, *et al*. T cell activation by antibody-like immunoreceptors: increase in affinity of the single-chain fragment domain above threshold does not increase T cell activation against antigen-positive target cells but decreases selectivity. *J Immunol* 2004;173:7647–53.
30 Intlekofer AM, Takemoto N, Kao C, *et al*. Requirement for T-bet in the aberrant differentiation of unhelped memory CD8+ T cells. *J Exp Med* 2007;204:2015–21.
31 Pritchard GH, Kedl RM, Hunter CA. The evolving role of T-bet in resistance to infection. *Nat Rev Immunol* 2019;19:398–410.
32 Zhong S, Malecek K, Johnson LA, *et al*. T-cell receptor affinity and avidity defines antitumor response and autoimmunity in T-cell immunotherapy. *Proc Natl Acad Sci U S A* 2013;110:6973–8.
33 Inderberg EM, Wälchli S. Long-term surviving cancer patients as a source of therapeutic TCR. *Cancer Immunol Immunother* 2020;69:859–65.
34 Stadtmauer EA, Fraietta JA, Davis MM, *et al*. CRISPR-engineered T cells in patients with refractory cancer. *Science* 2020;367:eaba7365.
35 Schober K, Voit F, Grassmann S, *et al*. Reverse TCR repertoire evolution toward dominant low-affinity clones during chronic CMV infection. *Nat Immunol* 2020;21:434–41.
36 Łuksza M, Riaz N, Makarov V, *et al*. A neoantigen fitness model predicts tumour response to checkpoint blockade immunotherapy. *Nature* 2017;551:517–20.
37 Eggermont AMM, Kicinski M, Blank CU, *et al*. Association between immune-related adverse events and recurrence-free survival among patients with stage III melanoma randomized to receive pembrolizumab or placebo. *JAMA Oncol* 2020;6:519–27.

SUPPLEMENTARY MATERIAL AND METHODS

Clinical course of the melanoma patient

A 56-year-old patient was diagnosed with malignant melanoma in 2008 and underwent resection of the primary tumor in the same year. In 2013 metastatic disease with pulmonary and intestinal metastases were detected. A biopsy from the lung metastasis (B_{Lung}) was performed for histologic confirmation of metastatic status of malignant melanoma. Subsequently, the patient underwent two cycles of chemotherapy resulting in a mixed response with regression of the intestinal metastasis (M_{Int}) but progression of lung metastasis (M_{Lung}). In November 2013, the patient became eligible for administration of anti-CTLA-4-antibody Ipilimumab for a total of four cycles. In March 2014, restaging revealed response of M_{Lung}, whereas M_{Int} progressed and was therefore surgically removed, together with two non-malignant lymph nodes (M_{Int}-LN1 and -LN2). The residual M_{Lung} previously targeted by biopsy, initially regressed, but later progressed and was therefore surgically removed in January 2016, together with one adjacent non-malignant lymph node (M_{Lung}-LN). Treatment with the PD-1-directed monoclonal antibody Pembrolizumab was subsequently applied for one year and the patient is in complete remission since then (Supplementary Fig. S1).

Cultivation of cell lines and primary human cells

All target cell lines were maintained in RPMI 1640, MEM or DMEM (Invitrogen), according to manufacturer's instructions, supplemented with Penicillin and streptomycin antibiotics (Pen/Strep), L-glutamine, non-essential amino acids (NEAA), sodium pyruvate (NaP) and 10% heat-inactivated fetal calf serum (FCS). T cells were cultured in RPMI supplemented with: L-glutamine, 5% human serum and 5% FCS, Hepes, Pen/Strep, NEAA, NaP and gentamycin.

T-cell antigen-experience recall responses

For stimulation with peptides, PBMCs were cultured as previously described[1 2]. Briefly, frozen PBMCs were thawed and cultured in AIM-V medium supplemented with 100 ng/ml of IL-4 and 100 ng/ml GM-CSF. After 24h, Poly:IC (20 µg/ml), IL-7 (0.5 ng/ml) and peptide pools (1 µM/peptide) were added to the culture. After 20-24h incubation, PBMCs were transferred on a pre-coated IFN-γ ELISpot plate, which was developed after additional 20-24h, prior transfer of PBMCs to culture for expansion of T cells in RPMI medium supplemented with IL-7 (5 ng/ml) and IL-15 (5 ng/ml) for 10-15 days. IFN-γ ELISpot assay was repeated on expanded T cells co-cultured for 72h with T2-A3 cells (E:T = 1:1) pulsed with single peptides from sub-pool A4 shared by Pool 4 and 9.

Arrangement of peptide pools for immunogenicity assessment of predicted ligands

The first 25 predicted binders to each allele were synthetized and used for stimulation assays, excluding previously identified neoantigens (NCAPG2^{P333L}, ranked 24th and SYTL4^{S363F} ranked 6th). In total 48 peptides were assembled in 11 pools. Each pool contained 10 peptides: 5 HLA-A03:01-predicted binders (sub-pool A) and 5 HLA-B27:05-predicted binders (sub-pool B) were arranged as depicted in Supplementary Table S3. Sub-pools A5 and B2 contained 9 peptides, due to the exclusion of known immunogenic peptides[1]. Pool 11 contained peptide SYTL4^{S363F} and served as positive control for peptide pool approach. Following screening of peptide pools, T cells were expanded for two weeks and co-cultured with single-peptide-pulsed target T2 cells to define the peptides eliciting reactivity in the pool.

IC_{50} in vitro measurement of predicted peptide candidates and neoantigens

Binding of selected peptides to HLA was further investigated through a peptide exchange assay. HLA-A03:01, HLA-B27:05, and human β2m (hβ2m) were expressed in E. coli and purified from inclusion bodies as described previously[3]. Purified proteins were stored at −80 °C until use. Folding of heavy chain–hβ2m–peptide complexes was performed by diluting purified denatured proteins to a final concentration of 30 µg/mL of heavy chain and 30 µg/mL hβ2m folding buffer (100 mM Tris·Cl, pH 7.5, 0.4 M arginine, 2 mM EDTA, 0.5 mM oxidized glutathione, 5 mM reduced glutathione, and 0.5 mM PMSF) and stirring at 4 °C (2 days for HLA-A03:01, 14 days for HLA-B27:05) with 10 µM high-affinity peptide (KLIETYFJK for HLA-A03:01, and RRKJRRWHL for HLA-B27:05, where J is the photolabile aa residue)[4]. After folding, samples were ultracentrifuged at 15,000 × g for 20 min and further purified by gel filtration. For peptide exchange reaction, 0.5 µM HLA class I monomers (HLA–hβ2m– photolabile peptide complex) were exposed to UV radiation (345 nm, 1000 W) for 5 min, followed by incubation for 18 h at 4 °C with 10nM fluorophore-labeled peptide (KLIE-FITC-YFSK for HLA-A3:01 and RRKW-FITC-RWHL for HLA-B27:05, FITC λex = 494 nm, λem = 517 nm) and varying concentration of the measured peptide. The binding was measured by fluorescence anisotropy using a Victor 3V reader (Perkin Elmer) in a black 96-well plate (Corning). Data were fitted and IC_{50} values were calculated by using GraphPad Prism 7.

TCR in situ hybridization

RNA in situ hybridization for identification of neoantigen-specific TCR on FFPE tumor slides was performed using BaseScope™ Detection Reagent Kit v2 - RED (ACD). TCR-specific Probes were designed to anneal on the TCR CDR3 sequence. Probes against PPIB (Cyclophilin B) and a bacterial protein (DapB, Bacillus subtillis) served as respective positive and negative controls. For each paraffin tumor block, slides of 4 µm were trimmed

with a microtome. Tissue slides were deparaffinized, pretreated using Protease IV (ACD) and stained with target probe, negative control and positive control probes following the manufacturer's instructions on an automated immunostainer. For localization of T-cell infiltration, Immunohistochemistry (IHC) was performed using anti-CD3-antibody (clone MRQ, Cell Marque Cat# 103R) as previously described[1]. Slides were scanned on a Leica AT2 (Leica, Wetzlar, Germany) system and visualized using Aperio ImageScope software (v12.4.3).

HLA-peptide complex structural modelling and SASA calculation

Each model was solvated in a rectangular box of TIP3P[5] water with a minimum distance of 12 Å between solute and box boundary, neutralized, and energy minimized. All modelling steps were performed using AMBER17[6]. The force field FF14SB was selected[7]. Subsequently, all 6 models were progressively heated up to 300 K over 3 ns gradually releasing initial positional restraints from the solute (Supplementary Table S4). The last heat-up step was performed in constant number, pressure and temperature (NPT) thermodynamic ensemble whereas the other steps were performed in constant number, volume and temperature (NVT). Temperature was controlled using a Langevin thermostat with a collision frequency (gamma_ln) of 4.00 ps^{-1}. Pressure was controlled using a Berendsen barostat[8] with default settings. SHAKE algorithm[9] was applied for all bonds including hydrogen atoms. Particle mesh Ewald (PME) method[10] was used to compute long range electrostatic interactions. A cut-off for non-bonded interactions of 12 Å was applied. After equilibration models were simulated for 200 ns at 300 K using the NPT ensemble with a 1 fs time step. For each model 3 replicas were simulated resulting in a cumulative simulation time of 600 ns per system.

To quantitatively analyse the HLA-p interface, solvent-accessable surface area (SASA) was calculated for each peptide residue and the electrostatic potential of the interaction surface

as previously described[11 12]. Briefly, frames were extracted every 200 ps from the last 180 ns of each replicon and analyzed. To select representative structures for visualization, frames were clustered, and central structure of the highest populated cluster was picked. The clustering was based on non-hydrogen peptide atoms using the hierarchical agglomerative algorithm with an epsilon of 2.0 and default settings. Trajectory processing and clustering was conducted with the CPPTRAJ[13] tool provided in AmberTools17[6]. Molecule images were generated using PyMOL (version 1.7.X, Schrödinger, LCC). Electrostatic potential was computed with PyMOL plugin APBS Tools 2.1[14] using default settings. Hydrogen bonds were identified using the VMD software HBonds plugin (version 1.2)[15].

Molecular cloning and retroviral transduction of TCRs, minigenes and HLA

TCR repertoire PCR analysis followed by Sanger sequencing was performed to determine variable alpha and beta chain usage of neoantigen reactive T-cell clones[16 17]. V-D-J rearrangements of complementarity-determining regions (CDR3) were investigated using IMGT/V-Quest (http://www.imgt.org/IMGT_vquest/vquest) and the complete sequences were in silico reconstructed with Ensembl database. TCR sequences were modified by in silico murinization, insertion of an additional cysteine bridge and codon optimization (BioCat)[18 19]. Optimized TCR constructs were retrovirally transduced in $CD8^+$ healthy donor derived T cells as described before and expanded for 7 to 10 days with IL-7 and IL-15 (5ng/mL; Peprotech) before functional characterization[16 20].

SYTL4 and NCAPG2 mutated and WT minigenes were cloned as previously described[1]. KIF2C minigenes were in silico designed, comprising 100 bp up- and downstream of mutated position, synthetized (Genscript) and cloned into pMP71 backbone. Additionally, tandem constructs were in silico designed, synthetized (Genscript) and cloned into the pMP71 backbone with single or tandem constructs for minigenes containing mutated

sequences of all three neoantigens and WT counterparts separated in two different vectors. All minigene vectors included a reporter gene dsRed ExpressII to allow sorting of transgenic cells. Neoantigen-coding and WT counterpart minigenes were transduced in different cell lines as LCL-1, U-698-M, A2058 and MDST8 as previously described[1] with small changes for adherent cell lines omitting RetroNectin (Clontech). LCL-1 was transduced with single minigenes, while other cell lines with tandem constructs, followed by single clone selection.

TCR beta and alpha chains as well as tandem constructs of minigenes were separated by a self-cleaving P2A element[16]. All vectors were amplified using NEB® 5-alpha Competent E. coli (New England BioLabs) and purified with NucleoBond® Xtra Midi/Maxi (Macherey-Nagel).

T2 were retrovirally transduced with the HLA restriction elements HLA-A03:01 and B27:05 as described before[16].

In-vitro cytotoxicity assessment

For monitoring of T-cell mediated killing in vitro, two different adherent cell lines were chosen according to the naturally expressed HLA allotypes. MDST8 cell line expressing HLA-B27:05 was selected for SYTL4^{S363F}-specific TCRs; A2058 expressing HLA-A03:01 for KIF2C^{P13L} and NCAPG2^{P333L}-specific TCRs. Killing assays were performed with impedance-based xCELLigence assays (ACEA BioSciences)[21]. Target cell culturing media was added to each well of 96 well E-Plates (ACEA Biosciences) for background impedance measurement[22]. Dissociated adherent target cells were seeded on E-Plate at different densities depending on the cell line (A2058 – 50,000/well; MDST8 – 20,000/well). Cell density on plates is measured within the RTCA MP instrument inside a cell culture incubator for 24h. For addition of T cells, data acquisition was paused and effector cells were added. Data recording was initiated immediately at 15-min intervals for the first 8 h

and then at 30-min intervals for remaining 16 h. Target cells only as well as target cells and non-transduced T cells served as controls. For calculation of percentage of cytolysis, the following formula was adopted: $Cytotoxicity\ (\%) = 100 - \left(\frac{CI_{TCR}}{CI_{ntd}}\right) \times 100$.

Activation/dysfunction patterns of stimulated and restimulated enriched TCR-transgenic T cells

A near-infrared fluorescent protein (iRFP) linked with a T2A element was cloned downstream of TCR constructs KIF2-PBC2 and SYTL4-TIL1 to allow for flow-cytometry based enrichment of TCR-transduced T cells. Retroviral transduction was performed as stated above and iRFP-positive T cells were sorted on a FACSAria III Cell Sorter (BD Biosciences). Sorted T cells were coincubated with minigene-transduced U-698-M in an E:T ratio of 1:1. To analyze repeated antigen exposure, transduced and enriched T cells were co-cultured with irradiated U-698-M expressing mutated tandem minigene (E:T = 1:1), fed with IL-7 and IL-15 (5 ng/ml each) every three days and restimulated with respective target cells after 11 days. For flow cytometry assessment, T cells were stained with anti-CD8, TCRmu and Zombie UV Fixable Viability Kit (BioLegend). Expression of activation/dysfunction markers was assessed using anti-PD-1-antibody (BioLegend, Cat# 329930) and, in combination with True-Nuclear Transcription Factor buffer set (BioLegend), anti-T-bet (BioLegend, Cat# 644816). Proliferation after 6 days of target stimulation was assessed with CellTrace Violet Cell Proliferation Kit, (ThermoFisher) according to the manufacturer's recommendations. Flow cytometry data acquisition and analysis was performed as stated in respective section within the main manuscript.

REFERENCES

1. Bassani-Sternberg M, Braunlein E, Klar R, et al. Direct identification of clinically relevant neoepitopes presented on native human melanoma tissue by mass spectrometry. *Nature Communications* 2016;7:13404. doi: 10.1038/ncomms13404
2. Martinuzzi E, Afonso G, Gagnerault MC, et al. acDCs enhance human antigen-specific T-cell responses. *Blood* 2011;118(8):2128-37. doi: 10.1182/blood-2010-12-326231 [published Online First: 2011/07/01]
3. Garboczi DN, Hung DT, Wiley DC. HLA-A2-peptide complexes: refolding and crystallization of molecules expressed in Escherichia coli and complexed with single antigenic peptides. *Proceedings of the National Academy of Sciences of the United States of America* 1992;89(8):3429-33. doi: 10.1073/pnas.89.8.3429 [published Online First: 1992/04/15]
4. Rodenko B, Toebes M, Hadrup SR, et al. Generation of peptide-MHC class I complexes through UV-mediated ligand exchange. *Nat Protoc* 2006;1(3):1120-32. doi: 10.1038/nprot.2006.121 [published Online First: 2007/04/05]
5. Jorgensen WL, Chandrasekhar J, Madura JD, et al. Comparison of simple potential functions for simulating liquid water. *The Journal of chemical physics* 1983;79(2):926-35.
6. D.A. Case, I.Y. Ben-Shalom, S.R. Brozell, et al. AMBER 2017, University of California, San Francisco. 2017
7. Maier JA, Martinez C, Kasavajhala K, et al. ff14SB: Improving the Accuracy of Protein Side Chain and Backbone Parameters from ff99SB. *J Chem Theory Comput* 2015;11(8):3696-713. doi: 10.1021/acs.jctc.5b00255 [published Online First: 2015/11/18]
8. Berendsen HJ, Postma Jv, van Gunsteren WF, et al. Molecular dynamics with coupling to an external bath. *The Journal of chemical physics* 1984;81(8):3684-90.
9. Ryckaert J-P, Ciccotti G, Berendsen HJ. Numerical integration of the cartesian equations of motion of a system with constraints: molecular dynamics of n-alkanes. *Journal of computational physics* 1977;23(3):327-41.
10. Salomon-Ferrer R, Gotz AW, Poole D, et al. Routine Microsecond Molecular Dynamics Simulations with AMBER on GPUs. 2. Explicit Solvent Particle Mesh Ewald. *J Chem Theory Comput* 2013;9(9):3878-88. doi: 10.1021/ct400314y [published Online First: 2013/09/10]
11. Karimzadeh H, Kiraithe MM, Kosinska AD, et al. Amino acid substitutions within HLA-B* 27-restricted T cell epitopes prevent recognition by hepatitis delta virus-specific CD8+ T cells. *Journal of virology* 2018;92(13):e01891-17.
12. Rognan D, Scapozza L, Folkers G, et al. Molecular dynamics simulation of MHC-peptide complexes as a tool for predicting potential T cell epitopes. *Biochemistry* 1994;33(38):11476-85.
13. Roe DR, Cheatham TE, 3rd. PTRAJ and CPPTRAJ: Software for Processing and Analysis of Molecular Dynamics Trajectory Data. *J Chem Theory Comput* 2013;9(7):3084-95. doi: 10.1021/ct400341p [published Online First: 2013/07/09]
14. Jurrus E, Engel D, Star K, et al. Improvements to the APBS biomolecular solvation software suite. *Protein Sci* 2018;27(1):112-28. doi: 10.1002/pro.3280 [published Online First: 2017/08/25]
15. Humphrey W, Dalke A, Schulten K. VMD: visual molecular dynamics. *J Mol Graph* 1996;14(1):33-8, 27-8. doi: 10.1016/0263-7855(96)00018-5 [published Online First: 1996/02/01]
16. Klar R, Schober S, Rami M, et al. Therapeutic targeting of naturally presented myeloperoxidase-derived HLA peptide ligands on myeloid leukemia cells by TCR-transgenic T cells. *Leukemia* 2014;28(12):2355-66. doi: 10.1038/leu.2014.131
17. Liang X, Weigand LU, Schuster IG, et al. A single TCR alpha-chain with dominant peptide recognition in the allorestricted HER2/neu-specific T cell repertoire. *J Immunol* 2010;184(3):1617-29. doi: 10.4049/jimmunol.0902155 [published Online First: 2010/01/01]
18. Kuball J, Dossett ML, Wolfl M, et al. Facilitating matched pairing and expression of TCR chains introduced into human T cells. *Blood* 2007;109(6):2331-8. doi: 10.1182/blood-2006-05-023069 [published Online First: 2006/11/04]

19. Scholten KB, Kramer D, Kueter EW, et al. Codon modification of T cell receptors allows enhanced functional expression in transgenic human T cells. *Clin Immunol* 2006;119(2):135-45. doi: 10.1016/j.clim.2005.12.009 [published Online First: 2006/02/07]
20. Audehm S, Glaser M, Pecoraro M, et al. Key Features Relevant to Select Antigens and TCR From the MHC-Mismatched Repertoire to Treat Cancer. *Front Immunol* 2019;10:1485. doi: 10.3389/fimmu.2019.01485 [published Online First: 2019/07/19]
21. Peper JK, Schuster H, Löffler MW, et al. An impedance-based cytotoxicity assay for real-time and label-free assessment of T-cell-mediated killing of adherent cells. *Journal of immunological methods* 2014;405:192-98.
22. Hamidi H, Lilja J, Ivaska J. Using xCELLigence RTCA Instrument to Measure Cell Adhesion. *Bio-protocol* 2017;7(24)

SUPPLEMENTARY FIGURE LEGENDS

Figure S1.
Clinical course of disease of the melanoma patient. He was diagnosed with malignant melanoma in 2008 and underwent resection of the primary tumor that year. In 2013, pulmonary and intestinal metastases were detected and a lung biopsy (B_{Lung}) was performed for histological analysis. Carboplatin and paclitaxel were administered, resulting in a mixed response of metastatic disease. The patient was subsequently treated with the anti-CTLA-4-antibody Ipilimumab. In 2014, the progressing abdominal lesion (M_{Int}) and two non-malignant lymph nodes (LNs) were surgically removed. In 2016, one primarily responding lung metastasis (M_{Lung}) progressed and was resected with one adjacent non-malignant LN. Treatment with Pembrolizumab was subsequently administered for 18 months. The patient is currently in complete remission without therapy. Analyses performed on tissue samples and time points of blood withdrawals are depicted.

Figure S2.
Detection of immunogenicity of predicted neoantigen KIF2C^{P13L} in autologous PBMCs of the melanoma patient. **A**, PBMCs derived from time point 925 were cultured in presence of IL-4 and GM-CSF following addition of Poly:IC, IL-7 and peptide pools (1 µM/peptide). After 24h, IFN-γ ELISpot assay was performed. **B**, IFN-γ ELISpot assay with T cells expanded after stimulation with Pool 4 and 9 (Supplemental Table 3). Expanded T cells were incubated with T2-A3 cells (E:T = 1:1) pulsed with single peptides of subpool A4 shared by Pool 4 and 9 for 72h. Subpool B4 containing peptides only present in Pool 4 but not Pool 9, served as negative control.

Figure S3.
Expression of transgenic neoantigen-specific TCRs on the surface of human CD8+ T cells assessed by TCRmu staining. Representative flow cytometry plots of single-cell suspension of TCR-transduced-CD8+ T cells stained (7-10 days after transduction) for CD8, TCRmu, and 7-AAD; the dot plots were gated on living cells (7-AAD-) and CD8-TCRmu+ T cells. The numbers in the gate represent the percentage of CD8+-T cells expressing the murinized TCR. Gates were set on the basis of isotype control for TCRmu-Ab, for each single TCR. Transduction efficiency was assessed for all transgenic T cells showing consistent results for the different TCR constructs.

Figure S4.
Expression of transgenic neoantigen-specific TCRs on the surface of $CD8^+$ T cells assessed by multimer staining. Representative flow cytometry plots show stainings with indicated multimers: HLA-B27:05-SYTL4 (**A**), HLA-A03:01-KIF2C (**B**) and HLA-A03:01-NCAPG2 (**C**). TCR-transduced-$CD8^+$ T cells were then stained for CD8 and 7-AAD; the dot plots were gated on living cells (7-AAD^-). The values in the gate represent the percentage of multimer-positive $CD8^+$-T cells. The quadrants were set on the basis of non-transduced T cells and isotype control. One representative out of three experiments with T cells from two different healthy donors is shown.

Figure S5.
Functional avidity of neoantigen-specific TCRs. Representative plots of IFN-γ secretion of TCR-transduced T cells upon stimulation with T2 target cells pulsed with titrated peptide concentrations of SYTL4^{S363F} (**A**), KIF2C^{P13L} (**B**) and NCAPG2^{P333L} (**C**). EC_{50} values of all experiments were calculated by fitting a non-linear curve and results are summarized in Fig. 1D.

Figure S6.
TCR-transduced CD8^{+} T cells mediate specific lysis of target cells expressing defined neoantigens. **A**, **B** and **C**, growth of target cells transduced with MUT/WT minigenes is monitored for ca. 24h (impedance measurement every 15 min) before addition of transgenic T cells to the culture and observation of cytolysis. MDST8MUT/WT cells were seeded at density 20,000/well and 40,000 TCR-T cells/well were added at time 0 (**A**). A2058MUT/WT cells were seeded at density 50,000/well and 100,000 TCR-T cells/well were added (**B** and **C**). Cell index values of target cell lines are depicted on left y axis. Percentage of target cell lysis, calculated on non-transduced T cell, is depicted on right y axis and indicated by the colored line. **D**, Comparison of cytolysis mediated by all TCRs. TCR transduction efficiency is indicated in the figure legend.

Figure S7.
Investigation of peptide-dependent and – independent HLA alloreactivity of neoantigen-specific TCR. Reactivity of all defined TCRs was tested to different LCLs expressing common HLA allotypes, pulsed with 1 µM mutated peptides SYTL4^{S363F}, KIF2C^{P13L} and NCAPG2^{P333L} (pLCL) in comparison to non-pulsed condition (LCL). All experiments were performed three times on two different healthy-donor-derived sets of transduced T cells showing consistent results. For co-cultures, E:T ratio was 1:1 and read-out consisted of IFN-γ secretion, assessed by ELISA on culture supernatants after 20h incubation

Figure S8.
Venn diagrams with distribution of TCR CDR3 sequences. **A**, Overlap of TCR CDR3 clonotypes obtained from TCR-β sequencing on B_{Lung}, M_{Int} and M_{Lung}. **B**, Overlap of TCR CDR3 clonotypes from removed metastases and associated lymph nodes. Arrows indicate shared compartments in which defined TCRs with validated neoantigen-specificity were detectable. The overlap was calculated using the Venn diagram tool from Bioinformatics & Systems Biology available online (http://bioinformatics.psb.ugent.be/webtools/ Venn/).

Figure S9.
RNA in situ hybridization of neoantigen-specific T cells within tumor tissue M_{Lung}. **A**, CDR3-specific probe visualizes T cells expressing TCR KIF2C-PBC2, which show polarization of detected RNA within single cells. **B**, anti-CD3 staining show an inhomogenous T-cell infiltrate. **C**, Negative control probe DapB (Bacillus subtillis). **D**, positive control probe Cyclophilin B.

Figure S10.
Expanded TIL from M_{Lung}^{1} were analyzed for specific responses against mutated peptide ligands. IFN-γ secretion upon stimulation with peptide-pulsed autologous LCL line and analyzed by IFN-γ ELISpot.

Figure S11.
Longitudinal monitoring of activation of TCR-transgenic T cells upon neoantigen encountering. **A-B**, percentage of T-bet positive cells within TCRmu^{+}CD8^{+} fraction of TCR-transduced T cells after 24 and 96 hours of co-culture with U-698-M expressing the mutated (**A**) or wildtype (**B**) tandem minigene. **C-D**, T-bet expression of SYLT4-TIL1-iRFP and KIF2C-PBC2-iRFP transduced T cells as shown in Fig. 6C including analysis after 96 hours after coincubation with mutated (**C**) or wildtype (**D**) transduced U-698-M.

SUPPLEMENTARY TABLES

Rank	Gene	Peptide seq (aa)	Mutation (aa)	Predicted affinity (nM)	Experimental IC_{50} (nM)
HLA-A03:01					
1	*CRMP1*	KIFNFYPRK	L > F	6.8	11.5
2	*FUT9*	KMKNFFFTK	S > F	7.4	135.7
3	*ANO7*	RMLRRRAQK	E > K	8.7	791.3
4	*ADAMDEC1*	TLYSPRGEK	E > K	9.2	416.9
5	*ASAH2*	AMYQRAKLK	S > L	9.5	27.1
6	*SLC5A3*	SLLTPPSTK	P > S	9.6	211.4
7	*CRYBB1*	RLMFFRPIK	S > F	9.8	57.6
8	*ZNF234*	SLYLKIHLK	L > K	11	--
9	*ZNF234*	KIYAAGTFY	H > Y	11.2	975
10	*DNAH5*	YLFFIQGYK	S > F	12.5	932.8
11	*TENM1*	TTYSPIGEK	G > E	14.5	81.51
12	*NCAPG2*	RLYKLILWR	P > L	14.7	707.1
13	*TGM5*	KTYPCKIFY	S > F	16.6	248.1
14	*FHDC1*	SLQPRGSFK	P > S	18.2	36.0
15	*CCDC7*	KVINLSPFK	E > K	18.6	474.3
16	*PCDHGA10*	CLFFGIPWK	S > I	19.2	2391
17	*SGK3*	KQFSAMALK	P > S	21.4	208.2
18	*KIF2C*	RLFLGLAIK	P > L	21.6	277.4
19	*AKAP6*	KLKLPIIMK	M > I	23.3	35.1
20	*FREM1*	LLINRGFSK	D > N	25.2	931.2
21	*UVSSA*	RLKCPFYGK	H > Y	26.1	249
22	*USP37*	KVMTDPSRK	A > V	28.7	16,29
23	*ARHGEF17*	RIAGKALKK	P > L	31.5	669
24	*NCAPG2*	KLILWRGLK	P > L	32.6	263.9
25	*ZFN226*	KLYQCNECK	S > L	32.7	3502

Table S1. Measured binding activity of top 25 neoantigen candidates for HLA-A03:01 predicted by NetMHC4.0.

Rank	Gene	Peptide seq (aa)	Mutation (aa)	Predicted affinity (nM)	Experimental IC_{50} (nM)
HLA-B27:05					
1	*TECTB*	R**R**FSSLYSF	G > R	11.5	48.0
2	*CLDN24*	RRLLILG**R**I	G > R	11.5	311.0
3	*KAT2A*	FRMF**L**TQGF	P > L	15	2.0
4	*TMPRSS11E*	ARWTA**F**FGV	S > F	17.1	525.0
5	*SDK2*	GRWALHSA**F**	S > F	17.5	68.0
6	*SYTL4*	GRIAF**F**LKY	S > F	18.4	224.0
7	*Ac087289.2, MRPL38, Ac087289.3*[a]	KRF**L**HRQPL	P > L	20.2	73.0
8	*B3GAT1*	A**R**FAVNLRL	G > R	20.7	8.0
9	*ITLN1*	WRNS**F**LLRY	S > F	24	29.0
10	*Af241726.2, CYBB*[a]	YR**I**YDIPPK	V > I	24	60.0
11	*KIF2C*	ARLF**L**GLAI	P > L	25.7	--
12	*P2RX1*	YRHLFKVF**R**	G > R	26.6	70.0
13	*SCN2A*	FRFFTR**K**SL	E > K	26.9	4.0
14	*RNF216*	RRHCRSY**N**R	D > N	27.6	55.0
15	*CLDN24*	KRRLLILG**R**	G > R	28.0	111.0
16	*ZFN234*	FRQSLYL**K**I	L > K	29.2	7.0
17	*NEK10*	RRTQRYFM**K**	E > K	29.3	46.0
18	*ERCC5*	FRI**C**PIFVF	R > C	32.3	877.0
19	*DSG1*	**K**RTNVGILK	E > K	33.3	136.0
20	*LIPH*	LRILR**I**KLR	M > I	35.6	109.0
21	*SI*	KR**H**EVPVPL	Y > H	36.8	907.0
22	*MBOAT1*	HRY**F**FFVAM	S > F	37.5	353.0
23	*SCN4A*	FRF**F**ATPAL	S > F	38.3	13.0
24	*INO80C*	LRFS**I**IEEF	T > I	45.9	--
25	*STON2*	SRVILF**S**PL	N > S	46.0	--

a) Overlapping genes

Table S2. Measured binding activity of top 25 neoantigen candidates for HLA-B27:05 predicted by NetMHC4.0.

Subpool A	A03:01 binders	Subpool B	B27:05 binders	Pools
A1	KIFN**F**YPRK	B1	R**R**FSSLYSF	Pool 1
	KMKNFF**F**TK		RRLLILG**R**I	
	RMLRRRAQ**K**		FRMF**L**TQGF	
	TLYSPRGE**K**		ARWTA**F**FGV	
	AMYQRAK**L**K		GRWALHSA**F**	
A2	SLLTPP**S**TK	B2	-	Pool 2
	RLM**F**FRPIK		KRF**L**HRQPL	
	SLYL**K**IHLK		A**R**FAVNLRL	
	KI**Y**AAGTFY		WRNS**F**LLRY	
	YL**F**FIQGYK		YR**I**YDIPPK	
A3	TTYSPIG**E**K	B3	ARLF**L**GLAI	Pool 3
	RLYK**L**ILWR		YRHLFKVF**R**	
	KTYPCKI**F**Y		FRFFTR**K**SL	
	SLQPRGSFK		RRHCRSY**N**R	
	KVINLSPF**K**		KRRLLILG**R**	
A4	CLFFG**I**PWK	B4	FRQSLYL**K**I	Pool 4
	KQF**S**AMALK		RRTQRYFM**K**	
	RLF**L**GLAIK		FRI**C**PIFVF	
	KLKLP**I**IMK		**K**RTNVGILK	
	LLI**N**RGFSK		LRILR**I**KLR	
A5	RLKCPF**Y**GK	B5	KR**H**EVPVPL	Pool 5
	K**V**MTDPSRK		HRY**F**FFVAM	
	RIAGKA**L**KK		FRF**F**ATPAL	
	-		LRFS**I**IEEF	
	K**L**YQCNECK		SRVILF**S**PL	
A1	KIFN**F**YPRK	B2	-	Pool 6
	KMKNFF**F**TK		KRF**L**HRQPL	
	RMLRRRAQ**K**		A**R**FAVNLRL	
	TLYSPRGE**K**		WRNS**F**LLRY	
	AMYQRAK**L**K		YR**I**YDIPPK	
A2	SLLTPP**S**TK	B3	ARLF**L**GLAI	Pool 7
	RLM**F**FRPIK		YRHLFKVF**R**	
	SLYL**K**IHLK		FRFFTR**K**SL	
	KI**Y**AAGTFY		RRHCRSY**N**R	
	YL**F**FIQGYK		KRRLLILG**R**	
A3	TTYSPIG**E**K	B4	FRQSLYL**K**I	Pool 8
	RLYK**L**ILWR		RRTQRYFM**K**	
	KTYPCKI**F**Y		FRI**C**PIFVF	
	SLQPRGSFK		**K**RTNVGILK	
	KVINLSPF**K**		LRILR**I**KLR	
A4	CLFFG**I**PWK	B5	KR**H**EVPVPL	Pool 9
	KQF**S**AMALK		HRY**F**FFVAM	
	RLF**L**GLAIK		FRF**F**ATPAL	
	KLKLP**I**IMK		LRFS**I**IEEF	
	LLI**N**RGFSK		SRVILF**S**PL	
A5	RLKCPF**Y**GK	B1	R**R**FSSLYSF	Pool 10
	K**V**MTDPSRK		RRLLILG**R**I	
	RIAGKA**L**KK		FRMF**L**TQGF	
	-		ARWTA**F**FGV	
	K**L**YQCNECK		GRWALHSA**F**	
A1	SLLTPP**S**TK	B2	GRIAF**F**LKY	Pool 11
	RLM**F**FRPIK		KRF**L**HRQPL	
	SLYL**K**IHLK		A**R**FAVNLRL	
	KI**Y**AAGTFY		WRNS**F**LLRY	
	YL**F**FIQGYK		YR**I**YDIPPK	

Table S3. Predicted peptide pool arrangement for immunogenicity assessment.

Step	Time (ps)	Restraint atoms	Restraint force constant (kcal mol-1 Å-2)	Initial temperature (K)	Target temperature (K)	Thermodynamic ensemble[d]	Barostat
1	10	all[a]	2.39	0	0	NVT	-
2	50	all[a]	2.39	2.5	5	NVT	-
3	50	all[a]	2.39	5	10	NVT	-
4	50	all[a]	2.39	10	20	NVT	-
5	50	bb[b]	2.39	25	50	NVT	-
6	100	bb[b]	2.39	50	100	NVT	-
7	100	bb[b]	2.39	100	200	NVT	-
8	100	bb[b]	0.24	100	200	NVT	-
9	200	mh-bb[c]	0.24	100	200	NVT	-
10	200	mh-bb[c]	0.24	150	300	NVT	-
11	590	-	-	150	300	NVT	-
12	1500	-	-	150	300	NPT	Berendsen

a) All MHC and peptide atoms
b) Heavy (C,CA,O,N) backbone (bb) atoms of MHC and peptide
c) Heavy backbone atoms of MHC (mh-bb)
d) NVT: constant number, volume and temperature; NPT: constant number, pressure and temperature

Table S4. Heat-up parameters used for MD simulations.

Name cell line	Alias	HLA-A	HLA-B	HLA-C
HOM2	LCL 01	03:01	27:05:00	01:02
SWEIG007	LCL 02	29:02:00	40:02:00	02:02
AMALA	LCL 03	02:17	15:01	03:03
OZB	LCL 04	02:09/03:01	35:01/38:01	04:01/12:03
RSH	LCL 05	68:02/30:01	42:01:00	17:01
KLO	LCL 06	02:08/01:01	50:01/08:01	07:01/06:02
LWAGS	LCL 07	33:01:00	14:02	08:02
-	LCL 08	02:01	07:02/15:01	30:4/12:03
BM21	LCL 09	01:01	41:01:00	17:01

Table S5. HLA-allotypes of lymphoblastoid cell lines

Table S6. Characteristics of neoantigen-specific TCRs.

Specificity	Source	TCR	TRAV	TRAJ	CDR3 alpha	TRBV	TRBJ	TRBD	CDR3 beta
SYTL4^{S363F}	TILs	SYTL4-TIL1	38-2/DV8*01	42*01	CAYRSARGSQGNLIF	7-8*01	2-5*01	2*01	CASSLGNYYQETQYF
		SYTL4-TIL2	35*02	52*01	CAAGGTSYGKLTF	27*01	2-3*01	2*01	CASSWGGAVGDTQYF
	PBMCs	SYTL4-PBC1	9-2*02	34*01	CALYTFYNTDKLIF	6-2*01	2-5*01	2*01	CASTIAASGYQETQYF
		SYTL4-PBC2	8-3*01	43*01	CAVGVLRGDMRF	12-3*01	2-3*01	1*01	CASSSRGPTDTQYF
KIF2C^{P13L}		KIF2C-PBC1	14/DV4*02F	31*01F	CAMREQNNNARLMF	7-6*01F	2-1*01F	2*01F	CASSLTRMGDRGEFF
		KIFC-PBC2	12-2*01F	6*01F	CAVKERASGGSYIPTF	10-3*02F	2-3*01F	1*01F	CAISDTSGGLWTDTQYF
NCAPG2^{P333L}		NCAPG2-PBC1	12-2*02	30*01	CPTGGDDKIIF	15*02	1-6*02	1*01	CATSRGDRPLHF

TCR	Recognition motif[a]	Number of antigens[b,c]
SYTL4-TIL1	X-R-I-A-F-F-X-X-X	6
SYTL4-TIL2	X-R-I-A-F-F-X-X-X	6
SYTL4-PBC1	X-R-I-A-F-F-X-X-X	6
SYTL4-PBC2	X-R-I-A-F-F-X-X-X	6
KIF2C-PBC1	X-X-X-L-X-L-A-I-K	60
KIF2C-PBC2	X-X-X-L-X-L-X-I-K	> 400
NCAPG2-PBC1	K-X-X-L-W-R-X-X-K	4

a) Recognition motifs are defined through T cell IFN-γ production in response to alanine/threonine scanned cognate epitopes
b) Number of human proteins containing matching recognition motif according to ScanProSite
c) Results derived from protein sequence database UniprotKB, Swiss-Prot (splice variants included)

Table S7. Number of human proteins potentially identified by neoantigen-specific TCR according to their recognition motif.

TCR	M_{Int} (%)	M_{Int}-LN1 (%)	M_{Int}-LN2 (%)	M_{Lung} (%)	M_{Lung}-LN (%)
SYTL4-TIL1	0.041	0.036	0.012	0.039	0.005
SYTL4-TIL2	0.079	0.022	0.019	0.017	0.026
SYTL4-PBC1	0.152	-	0.019	0.024	0.034
SYTL4-PBC2	0.029	0.014	-	0.020	0.021
KIF2C-PBC1	0.560	0.029	0.037	0.629	0.023
KIF2C-PBC2	0.115	0.007	0.019	0.800	0.070
NCAPG2-PBC1	0.003	0.007	-	-	-

Table S8. Productive frequency (%) of neoantigen-specific clonotypes in tumor metastases and lymph nodes detected by TCR-β sequencing.

TCR	d142 (%)	d546 (%)	d796 (%)	d945 (%)	d1120 (%)	d1519 (%)
SYTL4-TIL1	0.0018	0.0016	0.0022	0.0020	0.0008	0.0010
SYTL4-TIL2	-	-	0.0015	0.0007	0.0008	0.0010
SYTL4-PBC1	0.0053	0.0132	0.0112	0.0099	0.0115	0.0094
SYTL4-PBC2	-	0.0008	0.0015	0.0007	0.0008	-
KIF2C-PBC1	0.1489	0.1672	0.3273	0.5449	0.4715	0.2505
KIF2C-PBC2	0.0132	0.0311	0.0509	0.0365	0.0376	0.0136
NCAPG2-PBC1	0.0247	0.0156	0.0187	0.0205	0.0230	0.0167

Table S9. Productive frequency (%) of neoantigen-specific clonotypes detected by TCR-β sequencing on peripheral blood collected at different time points indicated as days (d) after start of Ipilimumab treatment.

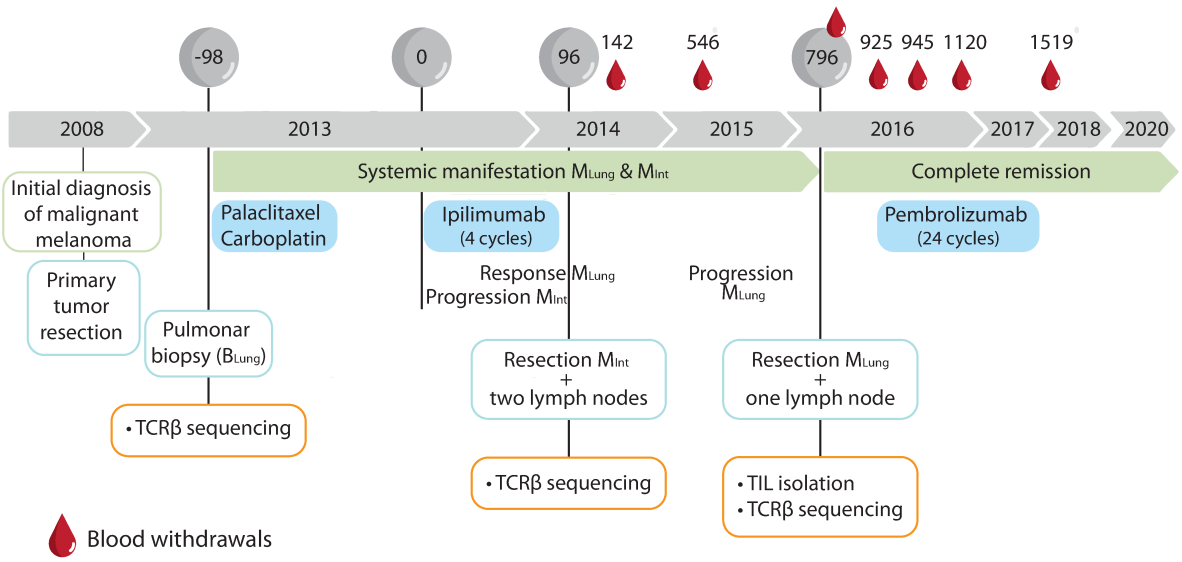
-98
0
96
142
546
796
925
945
1120
1519
2008
2013
2014
2015
2016
2017
2018
2020
Systemic manifestation MLung & MInt
Complete remission
Initial diagnosis of malignant melanoma
Primary tumor resection
Palaclitaxel Carboplatin
Pulmonar biopsy (BLung)
• TCRβ sequencing
Ipilimumab (4 cycles)
Response MLung
Progression MInt
Resection MInt + two lymph nodes
• TCRβ sequencing
Progression MLung
Resection MLung + one lymph node
• TIL isolation
• TCRβ sequencing
Pembrolizumab (24 cycles)
Blood withdrawals

Figure S1

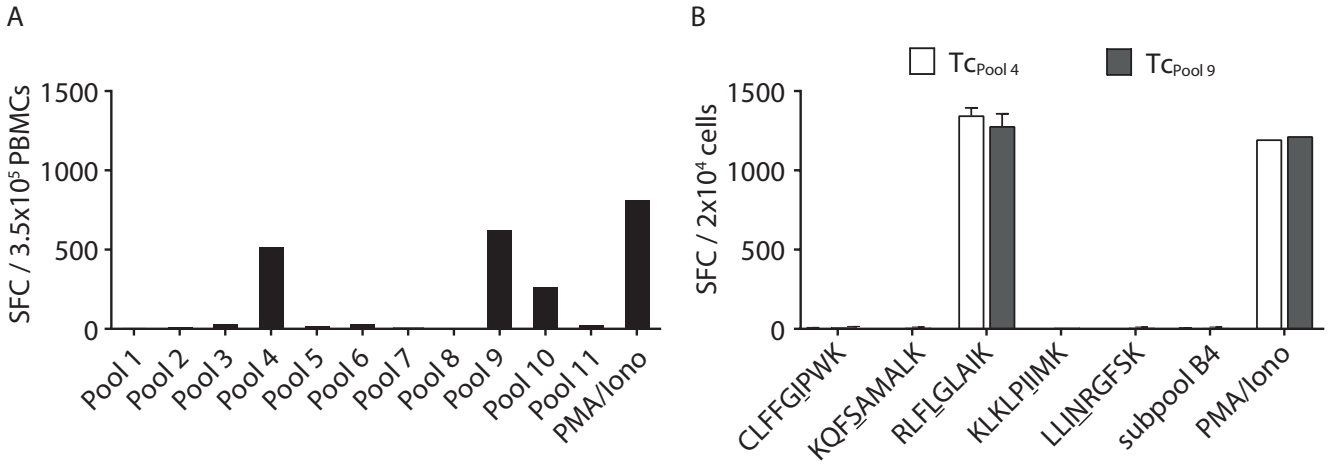
A
SFC / 3.5x10^5 PBMCs
1500
1000
500
0
Pool 1
Pool 2
Pool 3
Pool 4
Pool 5
Pool 6
Pool 7
Pool 8
Pool 9
Pool 10
Pool 11
PMA/Iono
B
TcPool 4
TcPool 9
SFC / 2x10^4 cells
1500
1000
500
0
CLFFGIPWK
KQFSAMALK
RLFLGLAIK
KLKLPIIMK
LLINRGFSK
subpool B4
PMA/Iono

Figure S2

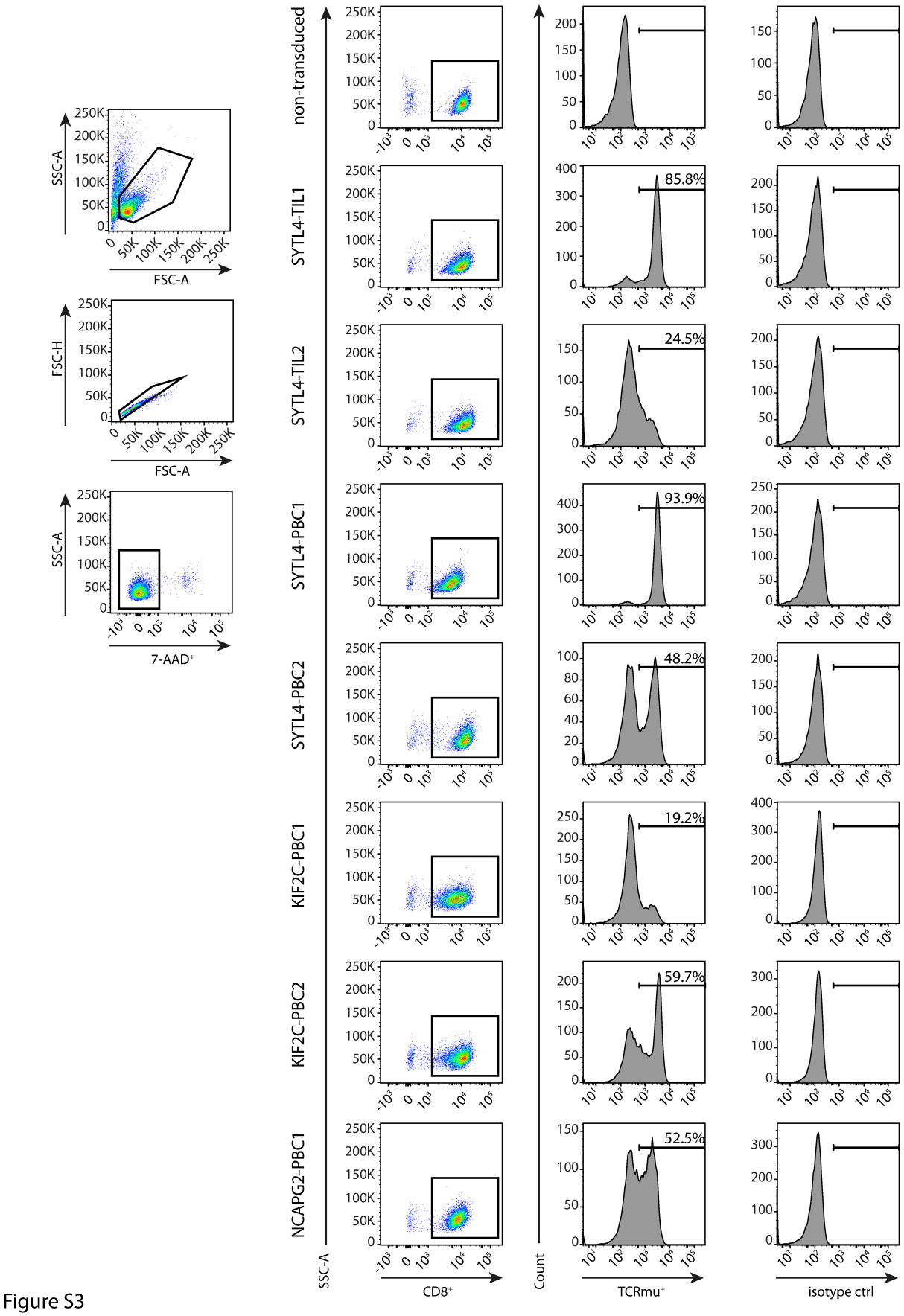
SSC-A
FSC-A
FSC-H
7-AAD+
non-transduced
SYTL4-TIL1
SYTL4-TIL2
SYTL4-PBC1
SYTL4-PBC2
KIF2C-PBC1
KIF2C-PBC2
NCAPG2-PBC1
85.8%
24.5%
93.9%
48.2%
19.2%
59.7%
52.5%
CD8+
Count
TCRmu+
isotype ctrl

Figure S3

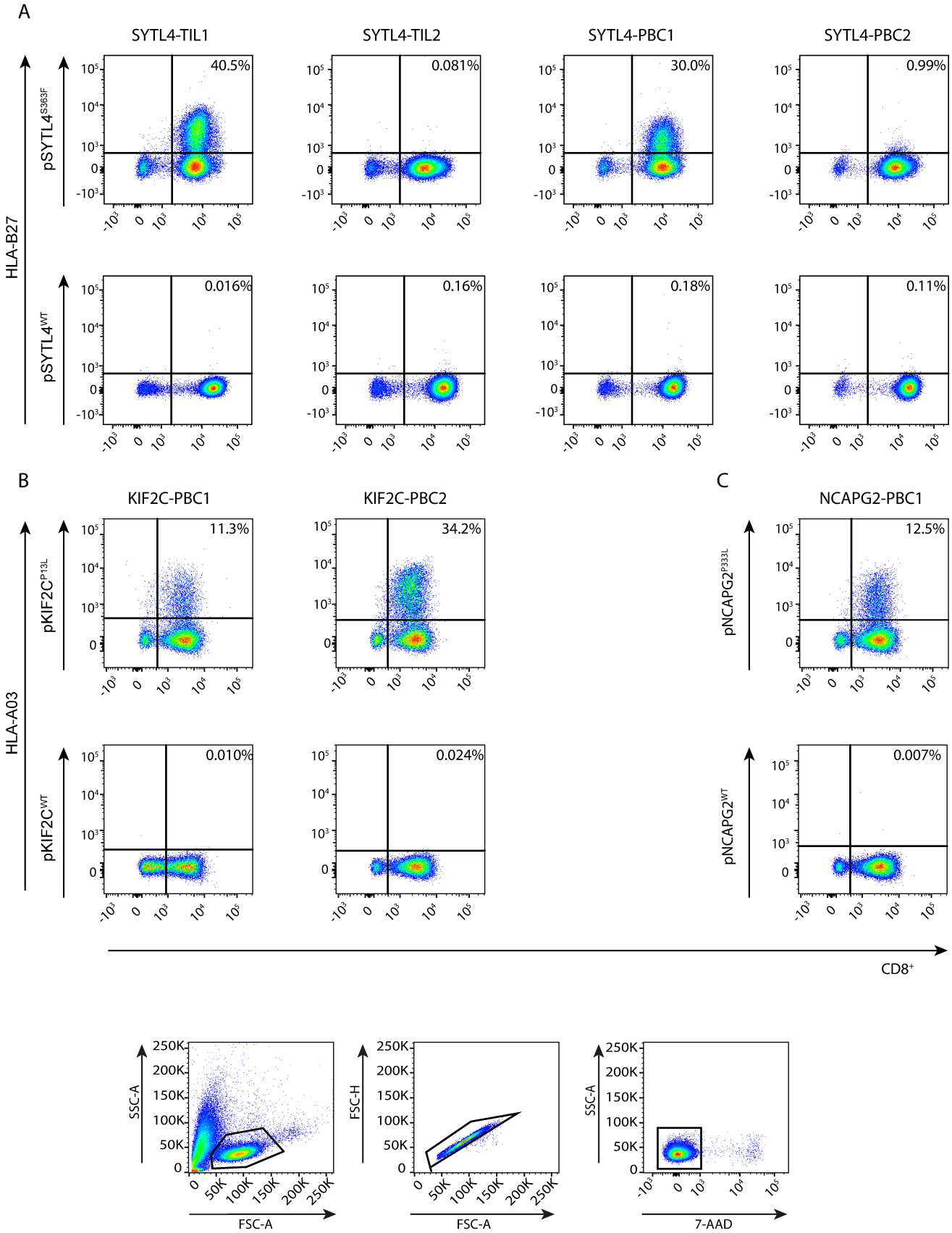
A
SYTL4-TIL1
SYTL4-TIL2
SYTL4-PBC1
SYTL4-PBC2
HLA-B27
pSYTL4S363F
pSYTL4WT
40.5%
0.081%
30.0%
0.99%
0.016%
0.16%
0.18%
0.11%
B
KIF2C-PBC1
KIF2C-PBC2
HLA-A03
pKIF2CP13L
pKIF2CWT
11.3%
34.2%
0.010%
0.024%
C
NCAPG2-PBC1
pNCAPG2P333L
pNCAPG2WT
12.5%
0.007%
CD8+
SSC-A
FSC-A
FSC-H
7-AAD

Figure S4

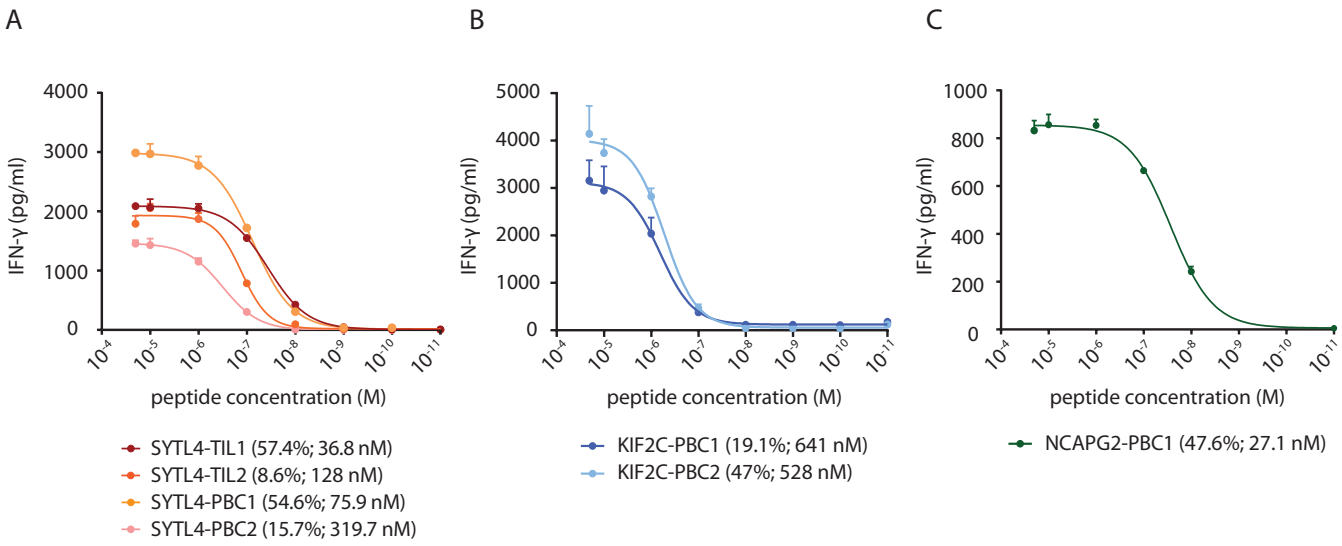
A
B
C
IFN-γ (pg/ml)
peptide concentration (M)
SYTL4-TIL1 (57.4%; 36.8 nM)
SYTL4-TIL2 (8.6%; 128 nM)
SYTL4-PBC1 (54.6%; 75.9 nM)
SYTL4-PBC2 (15.7%; 319.7 nM)
KIF2C-PBC1 (19.1%; 641 nM)
KIF2C-PBC2 (47%; 528 nM)
NCAPG2-PBC1 (47.6%; 27.1 nM)

Figure S5

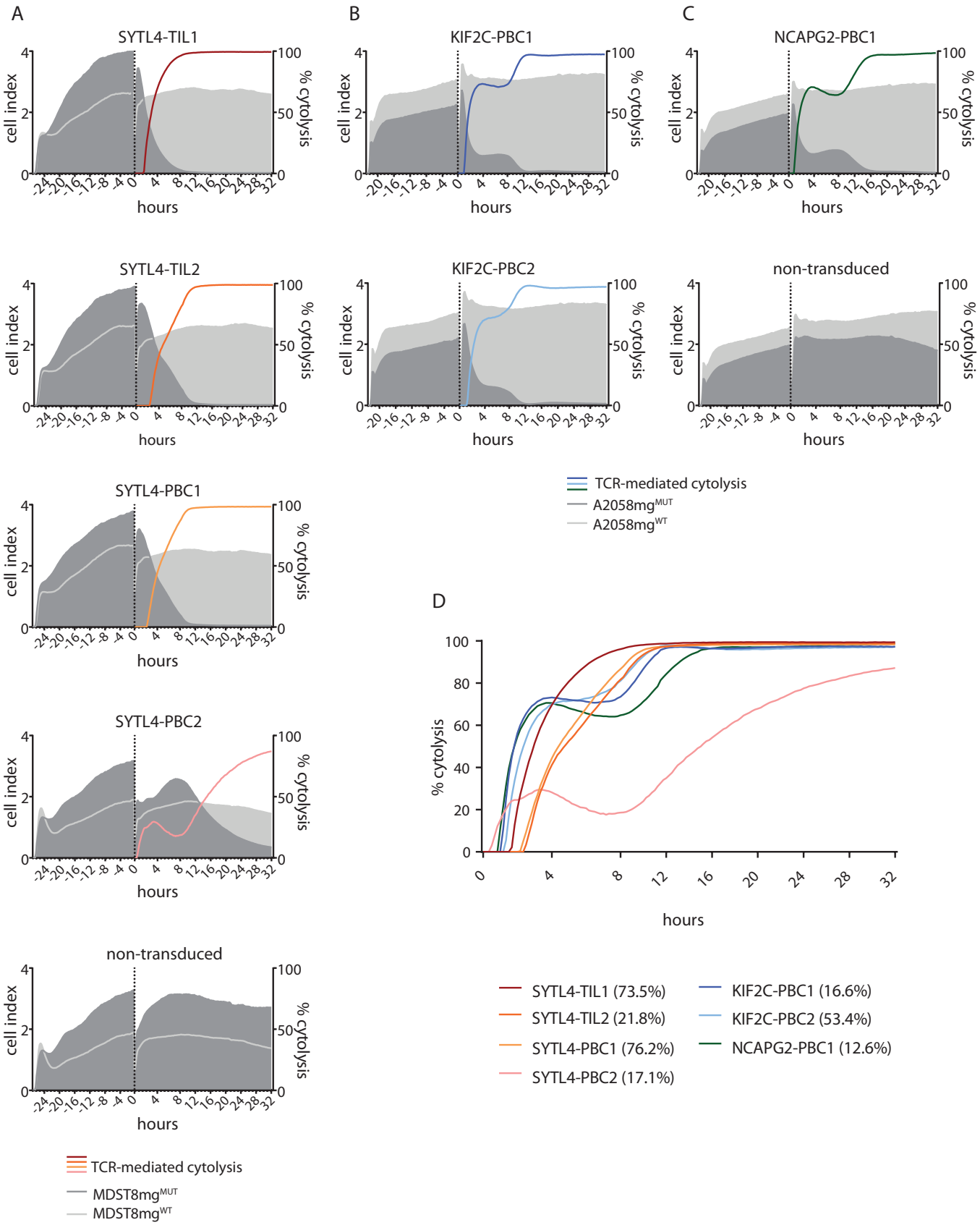
A
SYTL4-TIL1
B
KIF2C-PBC1
C
NCAPG2-PBC1
SYTL4-TIL2
KIF2C-PBC2
non-transduced
SYTL4-PBC1
SYTL4-PBC2
non-transduced
cell index
% cytolysis
hours
TCR-mediated cytolysis
A2058mg^MUT
A2058mg^WT
MDST8mg^MUT
MDST8mg^WT
D
% cytolysis
hours
SYTL4-TIL1 (73.5%)
SYTL4-TIL2 (21.8%)
SYTL4-PBC1 (76.2%)
SYTL4-PBC2 (17.1%)
KIF2C-PBC1 (16.6%)
KIF2C-PBC2 (53.4%)
NCAPG2-PBC1 (12.6%)

Figure S6

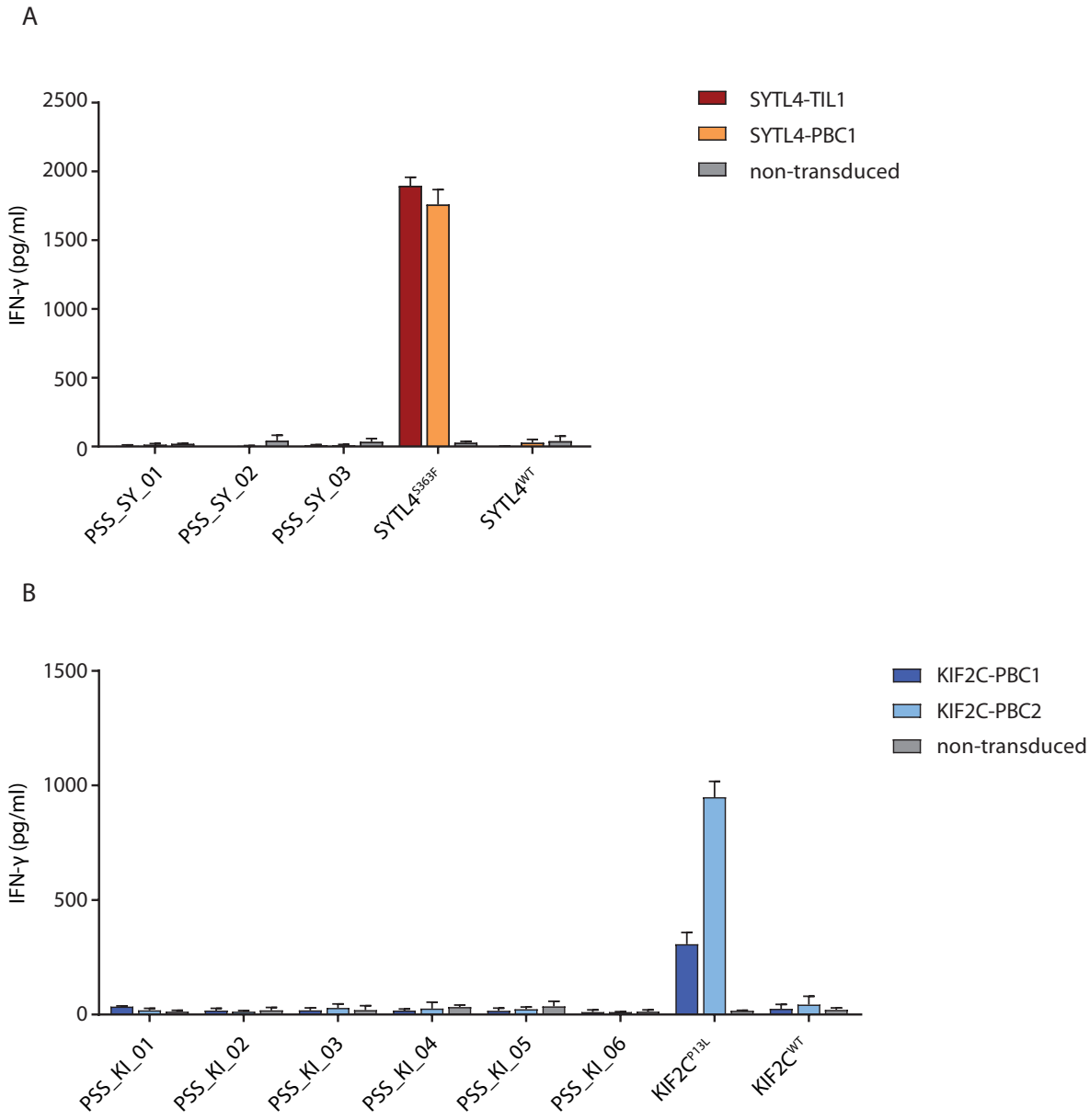
A
2500
2000
1500
1000
500
0
IFN-γ (pg/ml)
SYTL4-TIL1
SYTL4-PBC1
non-transduced
PSS_SY_01
PSS_SY_02
PSS_SY_03
SYTL4S363F
SYTL4WT
B
1500
1000
500
0
IFN-γ (pg/ml)
KIF2C-PBC1
KIF2C-PBC2
non-transduced
PSS_KI_01
PSS_KI_02
PSS_KI_03
PSS_KI_04
PSS_KI_05
PSS_KI_06
KIF2CP13L
KIF2CWT

Figure S7

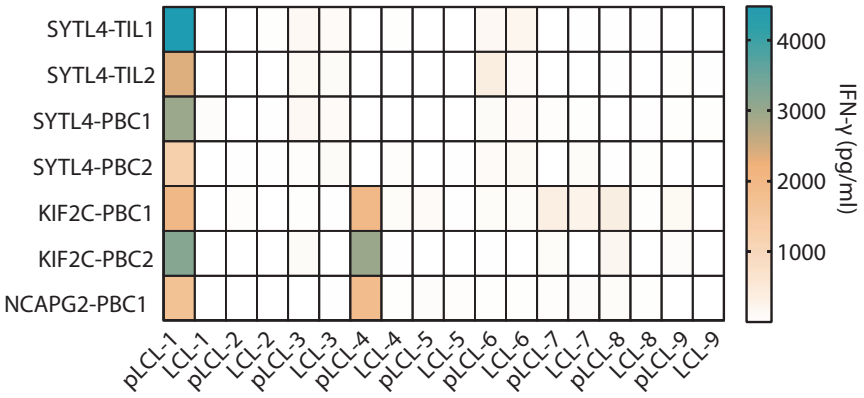
SYTL4-TIL1
SYTL4-TIL2
SYTL4-PBC1
SYTL4-PBC2
KIF2C-PBC1
KIF2C-PBC2
NCAPG2-PBC1
pLCL-1
LCL-1
pLCL-2
LCL-2
pLCL-3
LCL-3
pLCL-4
LCL-4
pLCL-5
LCL-5
pLCL-6
LCL-6
pLCL-7
LCL-7
pLCL-8
LCL-8
pLCL-9
LCL-9
4000
3000
2000
1000
IFN-γ (pg/ml)

Figure S8

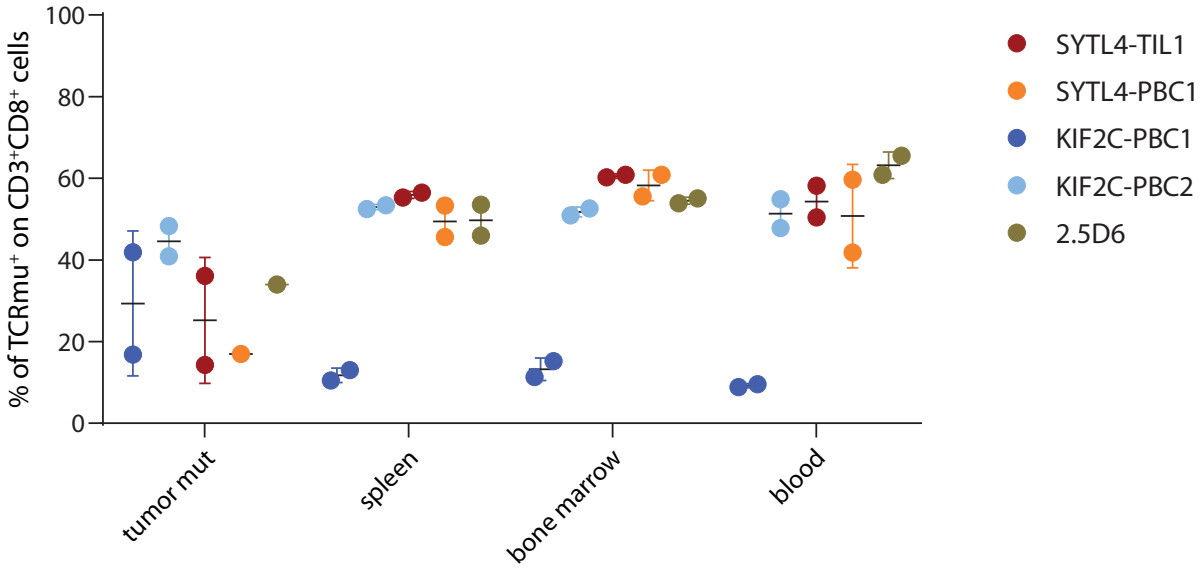
% of TCRmu+ on CD3+CD8+ cells
100
80
60
40
20
0
tumor mut
spleen
bone marrow
blood
SYTL4-TIL1
SYTL4-PBC1
KIF2C-PBC1
KIF2C-PBC2
2.5D6

Figure S9

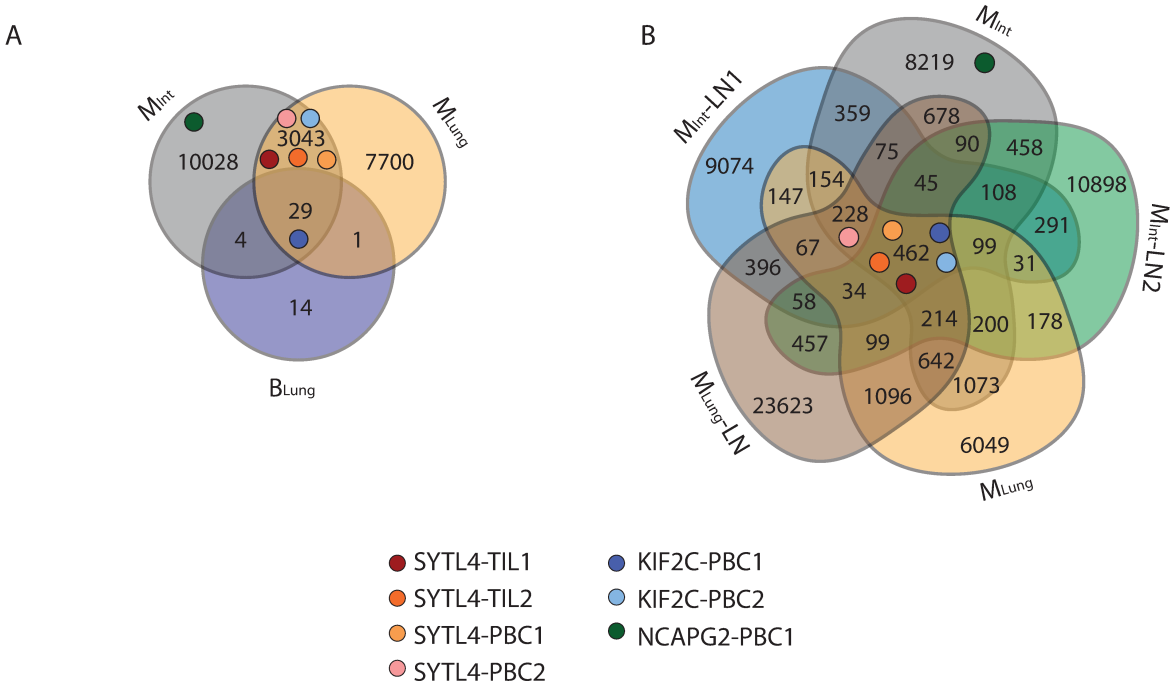
A
MInt
MLung
BLung
10028
3043
7700
29
4
1
14
B
MInt
MInt-LN1
MInt-LN2
MLung-LN
MLung
8219
359
678
90
458
9074
75
45
108
10898
154
147
228
291
67
462
99
31
396
34
58
214
200
178
457
99
642
1073
23623
1096
6049
SYTL4-TIL1
SYTL4-TIL2
SYTL4-PBC1
SYTL4-PBC2
KIF2C-PBC1
KIF2C-PBC2
NCAPG2-PBC1

Figure S10

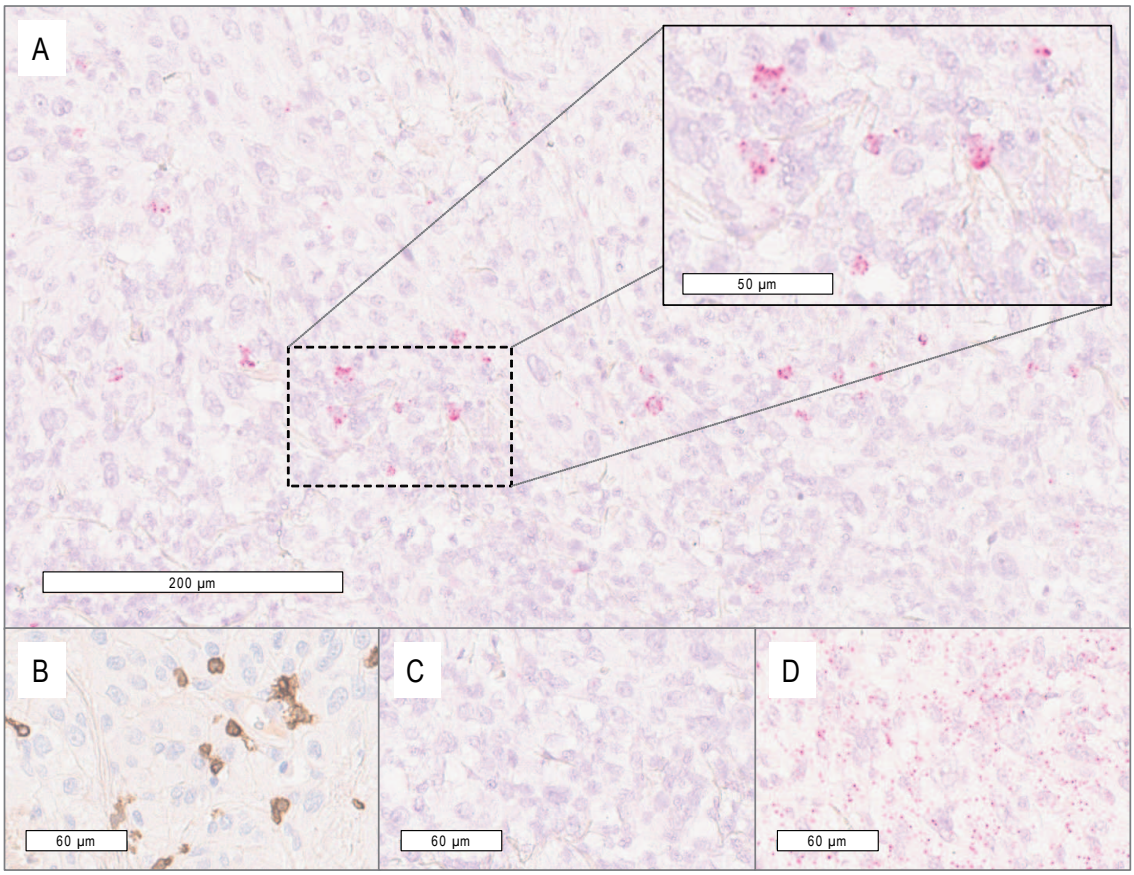

Figure S11

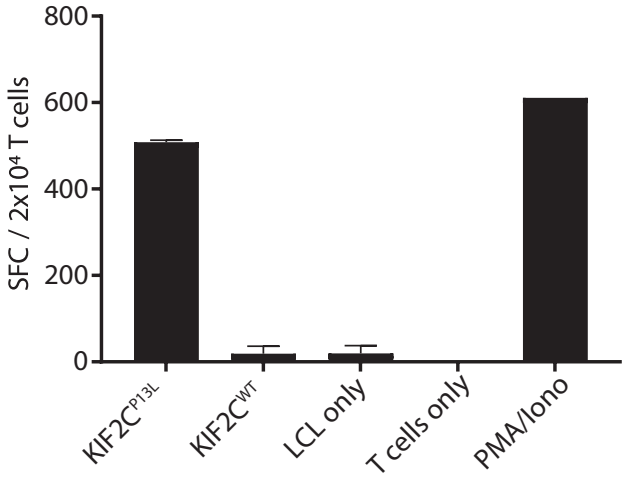
800
600
400
200
0
SFC / 2x10⁴ T cells
KIF2C^P13L
KIF2C^WT
LCL only
T cells only
PMA/Iono

Figure S12

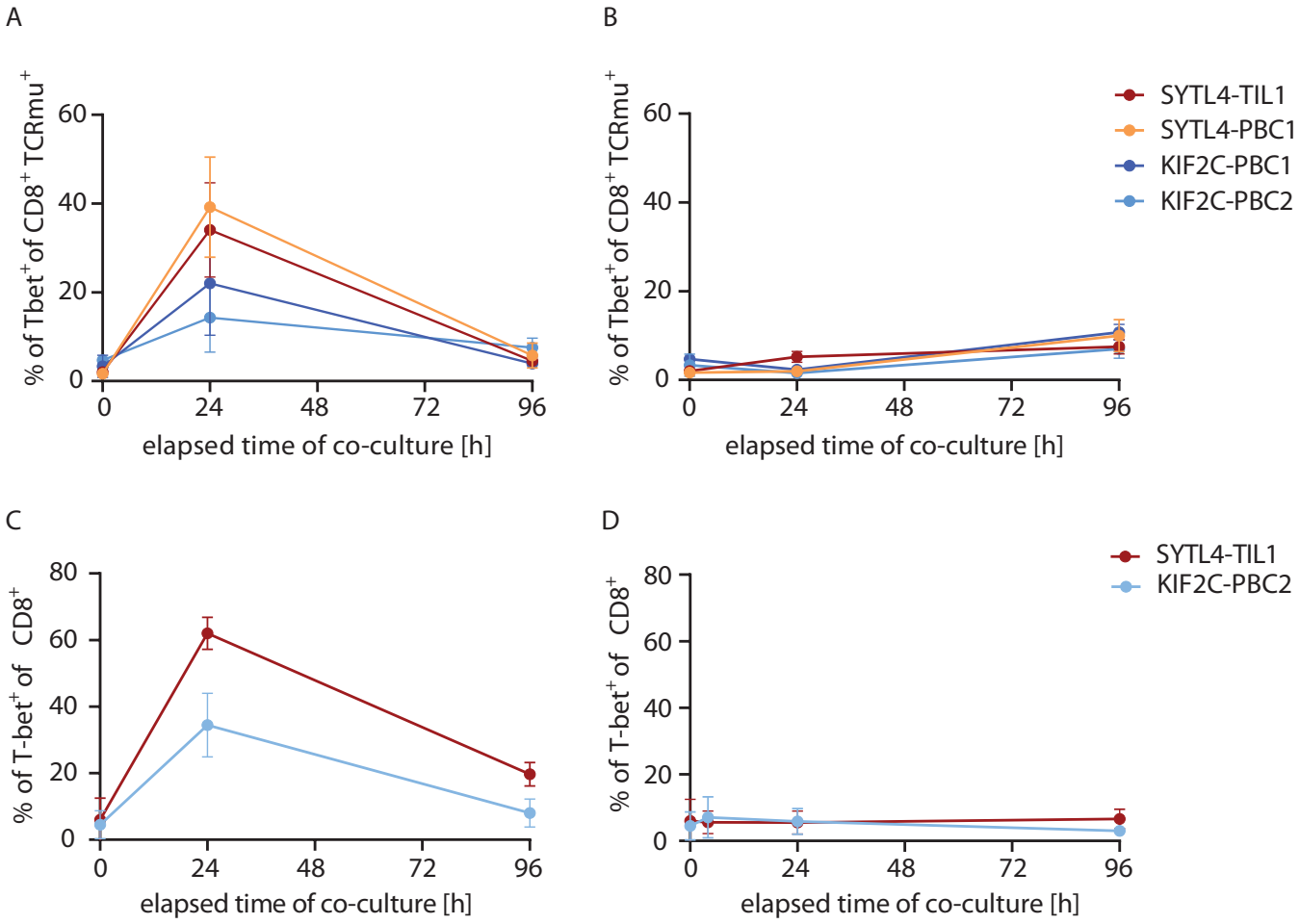
A
B
C
D
% of Tbet+ of CD8+ TCRmu+
% of T-bet+ of CD8+
elapsed time of co-culture [h]
SYTL4-TIL1
SYTL4-PBC1
KIF2C-PBC1
KIF2C-PBC2
0
20
40
60
80
0
24
48
72
96

Figure S13